Glutamatergic neuronal activity regulates angiogenesis and blood-retinal barrier maturation via Norrin/β-catenin signaling

Saptarshi Biswas[1,*], Sanjid Shahriar[2, 3], Galina Bachay[4], Panos Arvanitis[5], William J. Brunken[4] and Dritan Agalliu[1, 2, *]

[1]Department of Neurology, Columbia University Irving Medical Center, New York, NY 10032, USA.

[2]Department of Pathology and Cell Biology, Columbia University Irving Medical Center, New York, NY 10032, USA.

[3]Wyss Institute for Biologically Inspired Engineering, Boston, MA 02115, USA.

[4]Department of Ophthalmology and Visual Sciences, SUNY Upstate Medical University, Syracuse, NY 13210, USA.

[5]Warren Alpert Medical School, Brown University, Providence, RI 02903, USA.

***Corresponding authors:**

Saptarshi Biswas Ph.D. Email – sb4082@cumc.columbia.edu

Dritan Agalliu Ph.D. Email – da191@cumc.columbia.edu

Lead contact:

Dritan Agalliu Ph.D. Email – da191@cumc.columbia.edu

Keywords:

Glutamate, neuronal activity, angiogenesis, blood-retinal barrier, tight junctions, Norrin/β-catenin signaling

SUMMARY

Interactions among neuronal, glial and vascular components are crucial for retinal angiogenesis and blood-retinal barrier (BRB) maturation. Although synaptic dysfunctions precede vascular abnormalities in many retinal pathologies, how neuronal activity, specifically glutamatergic activity, regulates retinal angiogenesis and BRB maturation remains unclear. Using *in vivo* genetic studies in mice, single cell RNA sequencing and functional validation, we show that deep plexus angiogenesis and paracellular BRB maturation are delayed in *Vglut1*$^{-/-}$ retinas, where neurons fail to release glutamate. In contrast, deep plexus angiogenesis and paracellular BRB maturation are accelerated in *Gnat1*$^{-/-}$ retinas, where constitutively depolarized rods release excessive glutamate. Norrin mRNA expression and endothelial Norrin/β-catenin activity are downregulated in *Vglut1*$^{-/-}$ retinas, and upregulated in *Gnat1*$^{-/-}$ retinas. Pharmacological activation of endothelial Norrin/β-catenin signaling in *Vglut1*$^{-/-}$ retinas rescued defects in deep plexus angiogenesis and paracellular BRB integrity. Our findings demonstrate that glutamatergic neuronal activity regulates retinal angiogenesis and BRB maturation by modulating Norrin/β-catenin signaling.

39 **INTRODUCTION**

40 The crosstalk among neuronal, glial, and vascular components is essential, not only for proper angiogenesis,
41 but also for the establishment of the inner blood-retinal barrier (BRB) in the developing retina (Klaassen et
42 al., 2013). Retinal angiogenesis is tightly coordinated with the maturation of the BRB properties by
43 endothelial cells (ECs), through the presence of tight-junctions (TJ) that limit paracellular permeability
44 between ECs, specialized transporters to facilitate bidirectional transport of nutrients, and suppression of
45 transcytosis that reduces transcellular EC permeability (Chow and Gu, 2015; Zhao et al., 2015). Although
46 multiple signaling pathways operating in ECs, pericytes (PCs), neuronal or glial cells have emerged as
47 critical regulators of retinal angiogenesis and BRB maturation [reviewed in (Biswas et al., 2020)], it is
48 unclear how distinct types of neuronal synaptic activities influence these processes, and whether
49 neurotransmitters act directly on ECs to mediate their effects. This is highly significant since early loss of
50 neurovascular coupling, impaired response of photoreceptors to light, gradual neurodegeneration, gliosis
51 and neuroinflammation are found prior to any obvious vascular pathologies in diabetic retinopathy and
52 other retinal disease (Abcouwer and Gardner, 2014; Pardue et al., 2014; Umino and Solessio, 2013).
53 Moreover, it has been postulated that diabetes-induced changes in neurons and glial cells lead to vascular
54 defects (Feit-Leichman et al., 2005); yet, the underlying mechanisms remain elusive.

55

56 Distinct types of neuronal activity are present in the postnatal mouse retina during angiogenesis and
57 BRB maturation **(Figure 1A)**. From birth to postnatal day (P) 10, starburst amacrine cells propagate a
58 spontaneous cholinergic wave (Bansal et al., 2000; Feller et al., 1996; Zhou, 1998). The cholinergic wave
59 then gradually subsides and a spontaneous glutamatergic wave emerges from P10 to P14 (Bansal et al.,
60 2000; Blankenship et al., 2009; Tiriac et al., 2018; Weiner et al., 2019). The majority of neuronal activity
61 in the mouse retina from P14 onwards is mediated by light-dependent glutamatergic synaptic activity of
62 photoreceptors, and photoactivation of intrinsically-photosensitive retinal ganglion cells (ipRGCs)
63 [reviewed in (Biswas et al., 2020)]. However, light activation of photoreceptors has been observed as early

64 as P8 (Bonezzi et al., 2018; Tiriac et al., 2018). The superficial vascular plexus develops between P0-P8
65 (Stahl et al., 2010) over the ganglion cell layer (GCL) synchronous with neural activity from the cholinergic
66 wave and photoactivation of ipRGCs. In contrast, the deep plexus (P8-P12) angiogenesis in the outer
67 plexiform layer (OPL) (Stahl et al., 2010) and BRB maturation span both cholinergic and glutamatergic
68 spontaneous waves, glutamatergic synaptic activity of photoreceptors as well as photoactivation of ipRGC
69 [reviewed in (Biswas et al., 2020)]. Few studies have addressed how neuronal activity regulates retinal
70 angiogenesis and BRB maturation in the developing retina. Photoactivation of both $Opn4^{+}$ (Rao et al., 2013)
71 and $Opn5^{+}$ (Nguyen et al., 2019) RGCs regulates angiogenesis in the retina. Pharmacological blockade of
72 cholinergic wave before P8 delays deep plexus angiogenesis and BRB maturation, suggesting an important
73 role for cholinergic activity in these processes (Weiner et al., 2019). However, the role of glutamatergic
74 neuronal activities in retinal angiogenesis and BRB maturation remains unclear, although this is the
75 predominant activity when most of the vascular development and maturation occurs in the retina.
76
77 The Norrin/β-catenin signaling is critical for retinal angiogenesis and BRB maturation by inducing
78 stabilization and nuclear translocation of β-catenin. Genetic elimination of Norrin (ligand), Frizzled-4,
79 Lrp5/6, Tspan12 (receptors) and β-catenin in the mouse retina delays superficial vascular plexus
80 angiogenesis, induces loss of the deep plexus (Junge et al., 2009; Luhmann et al., 2005; Xia et al., 2010;
81 Ye et al., 2009; Zuercher et al., 2012) and BRB integrity (Paes et al., 2011; Wang et al., 2012). How Norrin
82 expression is regulated in the retina remains unclear. Using *in vivo* anatomical and functional
83 characterizations of the vasculature, as well as single-cell transcriptomic analyses and validation studies,
84 we show that deep plexus angiogenesis and paracellular BRB maturation are delayed in *Vglut1*$^{-/-}$ retinas
85 that have reduced synaptic release of glutamate from photoreceptors and bipolar cells (Blankenship et al.,
86 2009). In contrast, deep plexus angiogenesis is accelerated and paracellular BRB matures precociously in
87 *Gnat1*$^{-/-}$ retinas, where rod photoreceptors remain constitutively depolarized due to the absence of the G
88 protein subunit α Transducin 1, critical for phototransduction (Calvert et al., 2000; Schroeder et al., 2018).

89 These phenotypes are not due to abnormalities in neurovascular unit (NVU) assembly, aberrant
90 specification of neuronal or glial subtypes, or changes in neuronal metabolic demand. Importantly, Norrin
91 mRNA expression in the inner nuclear layer (INL), and as a consequence endothelial Norrin/β-catenin
92 signaling, are downregulated in *Vglut1*$^{-/-}$ retinas, and upregulated in *Gnat1*$^{-/-}$ retinas. Pharmacological
93 activation of endothelial Norrin/β-catenin signaling in *Vglut1*$^{-/-}$ retinas rescues defects in both deep plexus
94 angiogenesis and paracellular BRB integrity. Our study elucidates a critical mechanism by which
95 glutamatergic neuronal activity regulates retinal angiogenesis and BRB maturation by modulating Norrin/β-
96 catenin signaling in the developing retina. These findings have important implications for development of
97 potential interventions in various neurovascular pathologies.
98
99 **RESULTS**
100 **Deep plexus angiogenesis is delayed in the *Vglut1*$^{-/-}$ retina.**
101 Photoreceptors release glutamate in the outer plexiform layer OPL in the dark and suppress
102 glutamate release upon photon capture (Okawa et al., 2008). The synaptic release of glutamate is dependent
103 on vGluT1, a vesicular glutamate transporter (Sherry et al., 2003). Consequently, *Vglut1*$^{-/-}$ mice have
104 reduced synaptic release of glutamate from photoreceptors and bipolar cells **(Figure 1B, C)**(Blankenship
105 et al., 2009). To understand if extracellular glutamate levels affect retinal angiogenesis, we compared the
106 vascular growth in both the superficial and deep plexuses between wild-type (WT) and *Vglut1*$^{-/-}$ retinas.
107 Since the central retina is developmentally more mature than the peripheral retina, we analyzed these two
108 regions separately **(Figure 1D)**. Although the vascular coverage of the retina in the superficial plexus was
109 similar in both genotypes by P8 and P10 **(Figure 1E-G)**, the vascular coverage of the retina in the deep
110 plexus and its branch-point density were reduced significantly in the *Vglut1*$^{-/-}$ retina at P10 and P12 **(Figure
111 1H-M)**. By P14, however, the vascular coverage of the retina in the deep plexus was similar between the
112 two genotypes, although the branch-point density of the *Vglut1*$^{-/-}$ deep plexus still remained significantly

113 lower than the WT **(Figure 1H-M)**. Importantly, these vascular deficit patterns were consistent in both the
114 central and peripheral retina of *Vglut1*$^{-/-}$ mice (**Figure 1I-M**).
115
116 To understand the molecular mechanisms underlying these vascular phenotypes, we performed
117 single-cell RNA-sequencing analyses (scRNA-seq) of retinal CD31^{+} ECs purified from dissociated P10
118 WT and *Vglut1*$^{-/-}$ retinas by fluorescence-activated cell sorting (FACS; **Figure S1A, B)**. The purity of ECs
119 was confirmed by uniform expression of EC markers [*Pecam1* (CD31) and *Cdh5* (VE-Cadherin)] in the
120 entire population, and absence of mural cell [*Pdgfrb* (PDGFRβ) and *Des* (Desmin)] and astrocyte [*Gfap*
121 and *Pdgfra*] markers **(Figure S1C)**. ECs isolated from P10 WT and *Vglut1*$^{-/-}$ retinas clustered separately on
122 the Uniform Manifold Approximation and Projection (UMAP) plot based on differences in their
123 transcriptomic signatures **(Figure 2A; Tables S1, S2)**. Gene ontology (GO) analyses of the differentially
124 expressed genes (DEGs) between the two genotypes revealed that pathways involved in angiogenesis, blood
125 vessel morphogenesis and cell proliferation were downregulated in P10 *Vglut1*$^{-/-}$ compared to WT retinal
126 ECs **(Figure 2B; Tables S3, S4, S7)**, consistent with the phenotypic data (**Figure 1**). In contrast, pathways
127 involved in cellular and protein metabolic processes were upregulated in P10 *Vglut1*$^{-/-}$ compared to WT
128 retinal ECs **(Figure 2C; Tables S3, S4, S6)**. Expression levels of several pro-angiogenic genes [e.g. *Ptprb*,
129 *Aplnr, Unc5b* etc.], including two effectors of Norrin/β-catenin pathway [*Ctnnb1* (β-catenin) and *Lef1*] were
130 downregulated significantly in P10 *Vglut1*$^{-/-}$ compared to WT retinal ECs **(Figure 2D, F; Table S3)**. In
131 contrast, the majority of genes enriched in the deep plexus tip cells (D-tip cells) compared to the superficial
132 plexus tip cells (S-tip cells) [e.g. *Bsg*, *Rgcc*, *Plxnd1*, *Cdkn1a*, *Pde4b*, *Prcp*], as well as those enriched in D-
133 tip cells compared to all ECs [e.g. *Lamb1*, *Pcdh17*, *Adm*] (Zarkada et al., 2021) were upregulated in P10
134 *Vglut1*$^{-/-}$ compared to WT retinal ECs **(Figure 2E, G; Table S4)**, indicative of a delay in angiogenic
135 processes at the transcriptome level. To validate these molecular findings, we labeled proliferating cells
136 with Ki67 in both WT and *Vglut1*$^{-/-}$ retinas to assess whether endothelial stalk cell proliferation was
137 downregulated in *Vglut1*$^{-/-}$ retinal ECs (**Figure 2H**) (Siemerink et al., 2013) . Consistent with the scRNAseq

138 data, there was a significant reduction in the number of proliferating Ki67^{+} ECs in P12 *Vglut1*$^{-/-}$ retinal deep
139 plexus compared to the WT **(Figure 2I, J)**, while the number of apoptotic ECs (cleaved Caspase-3^{+}) was
140 not significantly different **(Figure 2J)**. These findings suggest that the delayed angiogenesis in *Vglut1*$^{-/-}$
141 retinal deep plexus is due, in part, to reduced EC proliferation. In addition, consistent with the scRNA-seq
142 data, we observed numerous Dll4^{+} tip cells (Hellstrom et al., 2007; Suchting et al., 2007) in the leading edge
143 of the *Vglut1*$^{-/-}$ deep plexus at P12, while the WT deep plexus was completely vascularized at this stage
144 **(Figure 2K, L)**. These data demonstrate that angiogenesis (EC proliferation) in the retinal deep, but not
145 superficial, plexus, is delayed with a larger number of tip cells when there is no extracellular glutamate
146 release by neurons in the *Vglut1*$^{-/-}$ retinas.
147
148 **Paracellular BRB maturation is impaired in the *Vglut1*$^{-/-}$ retina.**
149 Next, we asked if diminished glutamate release from photoreceptors and bipolar cells affects BRB
150 maturation. We injected intravenously biocytin-tetramethylrhodamine (biocytin-TMR, 870 Da) tracer in
151 WT and *Vglut1*$^{-/-}$ mice at P10 and P14 and quantified its leakage in the retina as a functional readout of the
152 paracellular BRB maturation **(Figure 3A)**(Biswas et al., 2022; Mazzoni et al., 2017). There was a
153 significantly higher biocytin-TMR leakage (area and intensity) in the *Vglut1*$^{-/-}$ compared to the WT retinas
154 at both time points **(Figure 3B-G)**. Importantly, these patterns were consistent in both the central and
155 peripheral retina, and the superficial and deep plexuses. Consistent with a delay in BRB maturation, our
156 scRNA-seq analyses showed that expression levels of most genes that promote BRB maturation were
157 downregulated in P10 *Vglut1*$^{-/-}$ compared to WT retinal ECs, including tight junction-associated genes
158 [*Cldn5* (Claudin-5) and *Tjp1* (ZO-1)], transporters [*Slc7a5* (Lat1), *Slc2a1* (Glut1) etc.,] and effectors of
159 Norrin/β-catenin pathway [*Ctnnb1* and *Lef1*] **(Figure 3H, I; Table S5)**. Surprisingly, expression levels of
160 *Ocln* (Occludin; tight junction protein), vBM proteins (Collagen IV, Laminin), BBB transcription factors
161 (e.g. *Foxq1*, *Foxf2*, *Zic3* etc.), or caveolar-related transport (*Cav-1*, *Cav-2*, *Cavin-1*, *Mfsd2a*) were
162 unaffected in P10 *Vglut1*$^{-/-}$ retinal ECs **(Tables S2, S5)**.

163

164 We validated if endothelial expression of tight junction proteins was reduced in the *Vglut1*$^{-/-}$ retina
165 by labeling the retinas with Claudin-5 and ZO-1. Consistent with the scRNA-seq data, there was a
166 significant reduction in Claudin-5 and ZO-1 protein localization to EC junctions in the P14 *Vglut1*$^{-/-}$
167 compared to the WT retina (**Figure 3J-M**). These patterns were consistent in both the superficial and deep
168 plexuses (**Figure 3L, M**). Importantly, these phenotypes were not caused by abnormalities in the NVU
169 assembly, as mural cell (PDGFRβ^{+}), glial endfeet (Aquaporin-4; Aqp-4^{+}) and vascular basement membrane
170 (vBM; Laminin and Collagen IV) coverage of retinal blood vessels were similar between the two genotypes
171 **(Figure S2)**.

172

173 We asked whether the lack of glutamate release by neurons affects also the transcellular BRB
174 maturation. We injected intravenously albumin-Alexa594 (MW= 60kDa), a protein that crosses the BRB
175 primarily through a transcellular route (Mazzoni et al., 2017) into P10 WT and *Vglut1*$^{-/-}$ mice and assessed
176 its extravasation into the retina. The tracer was largely confined within the blood vessels in both genotypes,
177 and its intensity in the parenchyma was very low and identical between the genotypes **(Figure S3A, B)**. In
178 addition, there was no difference in endogenous serum IgG leakage between P10 WT and *Vglut1*$^{-/-}$ retinas
179 **(Figure S3C)**. These functional studies are consistent with the scRNAseq data showing no change in the
180 expression of *Mfsd2a*, required for suppression of transcellular BRB permeability (Chow and Gu, 2017),
181 between the two genotypes **(Table S2)**. In addition, immunofluorescence analysis showed no difference in
182 retinal EC expression of Caveolin-1, a transmembrane protein responsible for endothelial transcytosis
183 (Biswas et al., 2020; Gu et al., 2014), between the two genotypes **(Figure S3D, E).** Finally, PLVAP
184 expression, a component of the diaphragms of EC fenestrae normally found in the immature BRB (Bosma
185 et al., 2018) **(Figure S3F)**, was absent in ECs from both genotypes despite a slight downregulation of *Plvap*
186 mRNA in P10 *Vglut1*$^{-/-}$ retinal ECs by scRNA-seq **(Figure 3H; Table S5)**. Together, these data demonstrate

187 that there is a delay in the paracellular, but not transcellular, BRB maturation in both the superficial and
188 deep plexuses in retinas with decreased extracellular glutamate **(Figure S3G)**.
189
190 **BRB maturation is accelerated in the absence of the cholinergic wave due to an early onset of**
191 **glutamatergic activity.**
192 During development, the cholinergic wave persists beyond P10 in the *Vglut1*$^{-/-}$ retina lacking
193 glutamatergic neuronal activity (Blankenship et al., 2009). Conversely, the glutamatergic wave begins
194 earlier (P8) than usual in the *Chrnb2*$^{-/-}$ retina where the cholinergic wave is abolished (Bansal et al., 2000).
195 It has been recently reported that pharmacological blockade of cholinergic waves before P8 delays deep
196 plexus angiogenesis and BRB maturation, suggesting an important role for cholinergic activity to promote
197 these processes in the developing retina (Weiner et al., 2019). However, our phenotypic analysis of the
198 *Vglut1*$^{-/-}$ retinal vasculature implies that the cholinergic wave by itself is not sufficient to induce paracellular
199 BRB maturation since it is very delayed in the *Vglut1*$^{-/-}$ retina through P14 (**Figure 3**). To test this
200 hypothesis, we examined paracellular BRB integrity in the *Chrnb2*$^{-/-}$ retina where cholinergic wave is
201 abolished and glutamatergic wave begins earlier (P8) than usual (Bansal et al., 2000) **(Figure 4A)**. There
202 was less biocytin-TMR leakage in the parenchyma **(Figure 4B-D),** and increased Claudin-5 coverage of
203 blood vessels **(Figure 4E, F)** in the P10 *Chrnb2*$^{-/-}$ retina compared to the WT, consistent with the idea that
204 the earlier onset of glutamatergic wave promotes a precocious BRB maturation in the *Chrnb2*$^{-/-}$ retina. These
205 data demonstrate that the glutamatergic neuronal activity, but not the cholinergic wave, is the primary driver
206 of paracellular BRB maturation in the developing retina.
207
208 **Deep plexus angiogenesis is accelerated and paracellular BRB is precociously mature in the *Gnat1*$^{-/-}$**
209 **retina.**
210 Phototransduction is a complex cascade, dependent in part on the G protein subunit α Transducin 1
211 (*Gnat1*). *Gnat1*$^{-/-}$ rod photoreceptors remain constitutively depolarized (Calvert et al., 2000; Schroeder et

212 al., 2018) with a consequent increase in glutamate release from rods **(Figure 5A, B)**. To understand how
213 excess glutamate release by rod photoreceptors affects retinal angiogenesis, we compared the vascular
214 growth of the retinal superficial and deep plexuses between the WT and *Gnat1*$^{-/-}$ retinas. While the vascular
215 coverage of the retina in the superficial plexus was similar between the two genotypes by P10 **(Figure 5C,**
216 **D)**, both the vascular coverage of the retina by the deep plexus, and its branch-point density were
217 significantly increased in the *Gnat1*$^{-/-}$ retina at this stage **(Figure 5E-J)**. However, the angiogenesis
218 phenotype was transient, and by P14 there was no difference between the two genotypes **(Figure 5F, G, I,**
219 **J; Figure S4A)**. Importantly, these patterns were similar in both the central and peripheral retina. Consistent
220 with the accelerated deep plexus angiogenesis phenotype seen in the P10 *Gnat1*$^{-/-}$ retina, there was an
221 increased EC proliferation (Ki67^{+} ECs) in the P10 mutant compared to the WT deep vascular plexus **(Figure**
222 **5K, L)**.
223
224 Next, we asked whether excess glutamate release by rod photoreceptors affects paracellular BRB
225 maturation. Measurements of biocytin-TMR leakage area and fluorescence intensity showed a reduction in
226 tracer leakage in *Gnat1*$^{-/-}$ compared to the WT retinas in the central and peripheral retinas and the superficial
227 and deep plexuses at P10 and P14 **(Figures 5M-O; S4B-D)**. Consistent with the functional data, there was
228 a significant increase in Claudin-5 protein localization at BRB tight junctions in the P10 *Gnat1*$^{-/-}$ retina
229 compared to the WT **(Figure 5P-R)**. Importantly, these patterns were uniform in both the superficial and
230 deep plexuses. These data demonstrate that retinal deep plexus angiogenesis is accelerated and paracellular
231 BRB integrity is precociously mature when there is excess glutamate released by the rods.
232
233 It is possible that differences in the specification of neuronal subtypes or Müller glia in either *Vglut1*$^{-}$
234 $^{/-}$ or *Gnat1*$^{-/-}$ retinas may be responsible for the vascular phenotypes related to angiogenesis and BRB
235 maturation seen in these mutants. To address this issue, we immunolabelled and quantified the number of
236 retinal neurons and Müller glia. There was no significant difference in the number of ganglion cells [NeuN^{+}

237 (Buckingham et al., 2008; Hajdu et al., 2019)], amacrine (except for a slight reduction in the *Vglut1*$^{-/-}$ retina)
238 and horizontal cells [Calbindin^{+} (Usui et al., 2015)], photoreceptors [measured by outer nuclear layer (ONL)
239 thickness] among the three genotypes **(Figure S5A-I)**. Similarly, the number of Müller glia, measured by
240 Sox9 labeling (Poche et al., 2008; Serjanov et al., 2018) was similar among WT, *Vglut1*$^{-/-}$ and *Gnat1*$^{-/-}$
241 retinas **(Figure S5J, K).** Therefore, the angiogenesis and BRB phenotypes seen in *Vglut1*$^{-/-}$ and *Gnat1*$^{-/-}$
242 retinas are not caused by defects in neuronal and glial cell type specification.
243
244 **Neurons and Müller glia in the inner nuclear layer of the retina respond to altered levels of**
245 **extracellular glutamate.**
246 To understand how extracellular glutamate concentration affects retinal angiogenesis and
247 paracellular BRB maturation, we first asked whether glutamate can act directly on retinal ECs. Our scRNA-
248 seq analyses of P10 and P14 WT retinal ECs revealed that neither ionotropic (*Grin1*, *Grin2b*, *Grin2d*,
249 *Gria1*), nor metabotropic (*Grm3*, *Grm5*, *Grm6*, *Grm7*, *Grm8*) glutamate receptor subunits are expressed in
250 retinal ECs at these time points **(Figure S6A).** Thus, the action of glutamate is unlikely to be directly on
251 retinal ECs. Analysis of a previously published scRNAseq database of all cell types from the P14 retina
252 (Macosko et al., 2015) showed that ionotropic and metabotropic glutamate receptor subunits are expressed
253 primarily by the inner nuclear layer (INL) neurons and Müller glia **(Figure S6B)**, suggesting that
254 extracellular glutamate could act on INL neurons and Müller glia.
255
256 To examine whether altered levels of extracellular glutamate are sensed by Müller glia in *Vglut1*$^{-/-}$
257 and *Gnat1*$^{-/-}$ retinas, we measured the expression levels of glutamine synthetase (GS) - an enzyme that
258 coverts glutamate to glutamine -, and Glutamate Aspartate Transporter [GLAST, or excitatory aminoacid
259 transporter 1 (EAAT-1)] - a glutamate transporter. These proteins are upregulated in Müller glia when
260 exposed to excess extracellular glutamate (Shen et al., 2004; Taylor et al., 2003). GS and GLAST protein
261 expression levels, measured by the mean fluorescence intensity, were downregulated in *Vglut1*$^{-/-}$, and

262 upregulated in *Gnat1*$^{-/-}$ retinas, compared to the WT levels **(Figure 6A-D)**. To determine whether altered
263 levels of extracellular glutamate are sensed by neurons in *Vglut1*$^{-/-}$ and *Gnat1*$^{-/-}$, we measured the expression
264 levels of Glutamate Transporter 1 [GLT-1, or excitatory aminoacid transporter 1 (EAAT-2)], a glutamate
265 transporter expressed primarily in retinal neurons (Harada et al., 1998), with expression regulated by the
266 extracellular glutamate (Russo et al., 2013). GLT-1 expression in INL neurons was downregulated in the
267 *Vglut1*$^{-/-}$, and upregulated in the *Gnat1*$^{-/-}$ retinas, compared to the WT **(Figure 6E-F)**. These findings
268 confirm that altered levels of extracellular glutamate, present in either *Vglut1*$^{-/-}$ or *Gnat1*$^{-/-}$ retinas, are sensed
269 by Müller glia and INL neurons. Importantly, altered levels of extracellular glutamate do not trigger Müller
270 cell gliosis in *Vglut1*$^{-/-}$ and *Gnat1*$^{-/-}$ retinas, as there was no upregulation of GFAP expression [a marker of
271 gliosis; (Hippert et al., 2015; Lee et al., 2021)] in Müller glia processes spanning multiple retinal layers
272 (**Figure S5L**). However, normal GFAP expression was detected in retinal astrocytes over the GCL
273 (colocalized with PDGFRα) in all genotypes **(Figure S6L, M)**.
274
275 Next, we asked whether alterations in neuronal metabolic demand may trigger the vascular
276 phenotypes in *Vglut1*$^{-/-}$ and *Gnat1*$^{-/-}$ retinas. We examined expression levels of hexokinase-2 (HK2) and
277 pyruvate kinase M-2 (PKM2), two key glycolytic enzymes that are readouts of neuronal metabolism (Cheng
278 et al., 2020), by Western blotting. The levels of these enzymes were similar in both P10 WT, *Gnat1*$^{-/-}$ and
279 *Vglut1*$^{-/-}$ retinas **(Figure S7A-L)**. Thus, alterations in extracellular glutamate levels caused by genetic
280 perturbations in the release of glutamate by neurons do not affect neuronal metabolic demand in the retina.
281
282 **Extracellular glutamate levels affect Norrin expression by retinal neurons and Müller glia and**
283 **endothelial Norrin/β-catenin signaling.**
284 Our scRNA-seq analyses revealed that expression levels of two Norrin/β-catenin signaling effectors
285 (*Ctnnb1* and *Lef1*) promoting angiogenesis and BRB maturation were downregulated in P10 *Vglut1*$^{-/-}$
286 compared to WT retinal ECs **(Figures 2D; 3H)**. Among seven key transcription factors (*Foxf2*, *Foxl2*,

287 *Foxq1*, *Lef1*, *Ppard*, *Zfp551* and *Zic3*) required for BBB maturation (Hupe et al., 2017), only *Lef1* was
288 downregulated significantly in P10 *Vglut1*$^{-/-}$ retinal ECs, suggesting a very specific effect on Norrin/β-
289 catenin signaling. To address changes in Norrin/β-catenin signaling, we examined *Norrin* (*Ndp*) mRNA
290 expression in *Vglut1*$^{-/-}$ and *Gnat1*$^{-/-}$ retinas by fluorescent *in situ* hybridization (FISH). *Ndp* mRNA
291 expression was drastically reduced in the INL layer of P10 *Vglut1*$^{-/-}$ retinas compared to the WT; in contrast,
292 its expression was highly upregulated in the INL of P10 *Gnat1*$^{-/-}$ retinas compared to the WT **(Figure 6G,**
293 **H)**. The upregulation of *Ndp* persisted in the INL of *Gnat1*$^{-/-}$ retinas through P14 **(Figure S7M)**. Consistent
294 with our observations, analysis of a previously published scRNAseq database (Macosko et al., 2015)
295 demonstrated that INL neurons (horizontal cells and a subset of amacrine and bipolar cells) and Müller glia
296 express high levels of *Norrin* mRNA and glutamate transporters [*Slc1a2* (GLT-1) and *Slc1a3* (GLAST)]
297 respectively (Macosko et al., 2015) **(Figure 6I)**. Taken together, these transcriptional data and the response
298 of the INL cells (neurons and Müller glia) to extracellular glutamate (i.e, changes in GS, GLAST, GLT-1
299 protein levels) in the *Vglut1*$^{-/-}$ and *Gnat1*$^{-/-}$ retinas (**Figure 6**), suggest that glutamate could directly act on
300 Müller glia and INL neurons to induce *Norrin* mRNA expression.
301
302 Next, we examined the activation of Norrin/β-catenin signaling pathway in *Vglut1*$^{-/-}$ and *Gnat1*$^{-/-}$
303 retinal ECs. We immunolabeled P14 WT, *Vglut1*$^{-/-}$ and *Gnat1*$^{-/-}$ retinal sections with Lef1 (an effector of
304 Norrin/β-catenin signaling) and quantified the number of Lef1^{+} ECs in both the superficial and deep
305 plexuses. There were significantly fewer Lef1^{+} ECs in the *Vglut1*$^{-/-}$ retina and significantly higher in the
306 *Gnat1*$^{-/-}$ retina compared to the WT **(Figure 7A, B)**. Interestingly, our scRNA-seq data suggest that none
307 of the downstream targets of VEGF-A signaling [*Nr4a2*, *Egr3*, *Igfbp3*, *Hlx1*, *Crem*, *Per1*, *Mef2c*, *Ccrl1*,
308 *Thbd*, *Ndrg1*, *Dnajb9*, *Mycn*; (Schweighofer et al., 2009)] were altered in *Vglut1*$^{-/-}$ retinal ECs **(Table S2)**.
309 Therefore, angiogenesis and BRB phenotypes in *Vglut1*$^{-/-}$ and *Gnat1*$^{-/-}$ retinas are likely driven by altered
310 Norrin/β-catenin signaling.
311

312 **Activation of endothelial Norrin/β-catenin signaling restores angiogenesis and BRB deficits in *Vglut1*-**
313 **/- mice.**

314 If angiogenesis and BRB phenotypes in *Vglut1*$^{-/-}$ and *Gnat1*$^{-/-}$ retinas are driven by altered Norrin/β-
315 catenin signaling, we hypothesized that activating Norrin/β-catenin signaling in retinal ECs should rescue
316 angiogenesis and BRB phenotypes in *Vglut1*$^{-/-}$ retinas. To test this hypothesis, we injected intraperitoneally
317 either BIO [(2*Z*,3*E*)-6-bromoindirubin-3-acetoxime, BIO-Acetoxime] that activates Wnt (Norrin)/β-catenin
318 signaling by inhibiting GSK-3β, or MeBIO [1-methyl-BIO], an analog of BIO with minimal activity against
319 GSK-3β (Corada et al., 2019) in WT and *Vglut1*$^{-/-}$ mice. There were significantly fewer Lef1^{+} ECs in the
320 MeBIO-treated *Vglut1*$^{-/-}$ retina compared to the MeBIO-treated WT retina; however, BIO-treatment
321 significantly increased the number of Lef1^{+} ECs in the *Vglut1*$^{-/-}$ retina compared to the MeBIO-treated
322 *Vglut1*$^{-/-}$ retina **(Figure S8)**. Importantly, we did not observe any Lef1^{+} nuclei outside the vasculature with
323 either treatment. These data confirm that BIO-treatment activated Norrin/β-catenin signaling specifically
324 in *Vglut1*$^{-/-}$ retinal ECs. Measurement of vascular coverage in the deep plexus revealed that while vascular
325 coverage was significantly lower in the MeBIO-treated *Vglut1*$^{-/-}$ retina compared to the MeBIO-treated WT
326 retina, BIO-treatment significantly increased vascular coverage by the deep plexus in the *Vglut1*$^{-/-}$ retina
327 nearly to the MeBIO-treated WT retinas **(Figure 7C-E)**. Similarly, measurement of Biocytin-TMR leakage
328 area and intensity revealed that while tracer leakage was significantly higher in the MeBIO-treated *Vglut1*-
329 /- retina compared to the MeBIO-treated WT retina, BIO-treatment significantly decreased tracer leakage in
330 the *Vglut1*$^{-/-}$ retina nearly to the MeBIO-treated WT levels **(Figure 7F-I)**. Thus, activation of endothelial
331 Norrin/β-catenin signaling was sufficient to rescue angiogenesis and BRB phenotypes in the *Vglut1*$^{-/-}$ retina.
332 These data strongly suggest that glutamate released by neurons regulates retinal angiogenesis and
333 paracellular BRB integrity by modulating Norrin expression in retinal neurons and Müller glia and
334 endothelial Norrin/β-catenin signaling.
335

336 **DISCUSSION**

337 Structural and functional abnormalities in neurons or glial cells precede vascular pathologies in
338 multiple CNS neurological diseases with prominent vascular involvement, including those in the retina. For
339 example, in diabetic retinopathy there is an early loss of neurovascular coupling, impaired response of
340 photoreceptors to light, gradual neurodegeneration, gliosis and neuroinflammation before any observable
341 vascular pathologies (Abcouwer and Gardner, 2014; Pardue et al., 2014; Umino and Solessio, 2013).
342 Moreover, the early phases of either age-related macular degeneration, or retinitis pigmentosa, characterized
343 by changes in synaptic activity and metabolic deficits in Müller glia (Jones et al., 2016a; Jones et al., 2016b;
344 Pfeiffer et al., 2016), may also affect blood vessel function leading to neurodegeneration. Although vascular
345 pathologies, including aberrant angiogenesis and BRB breakdown, are found in diabetic retinopathy and
346 proliferative vitreoretinopathy that cause acquired adult blindness, as well as retinopathy of prematurity
347 which leads to blindness in premature infants (Chan-Ling and Stone, 1992; Klaassen et al., 2013; Liegl et
348 al., 2016; Prokofyeva and Zrenner, 2012), the molecular mechanisms that link neuronal or glial
349 abnormalities with vascular deficits remain elusive. Our studies elucidate a critical missing step that links
350 glutamatergic neuronal activity with vascular development and maturation in the retina, that may also be
351 highly relevant for several retinal disease. Below, we discuss: a) the role of glutamate in angiogenesis and
352 barriergenesis, b) the signaling pathways that function downstream of glutamate to promote these processes,
353 and c) the relevance for the disease.

354

355 Glutamate is the predominant neurotransmitter in the retina during vascular development and in
356 adulthood (Boccuni and Fairless, 2022). In our study, we used three mouse models: a) *Vglut1*$^{-/-}$, where
357 retinal photoreceptors and bipolar cells fail to release glutamate into the synaptic cleft, b) *Gnat1*$^{-/-}$, where
358 depolarized rod photoreceptors release excess glutamate into the synaptic cleft, and c) *Chrnb2*$^{-/-}$, where
359 cholinergic wave is abolished but glutamatergic wave begins at P8 instead of P10 to address its role in
360 angiogenesis and barriergenesis. We found that deep plexus angiogenesis and paracellular BRB maturation

361 in the retina are critically linked to the extracellular glutamate levels. These processes are delayed in *Vglut1*$^{-}$
362 $^{/-}$ retinas, where neurons fail to release glutamate. In contrast, deep plexus angiogenesis and paracellular
363 BRB maturation are accelerated in *Gnat1*$^{-/-}$ retinas, where constitutively depolarized rods release excessive
364 glutamate. Although the deep plexus angiogenesis, which occurs from P8-P12, was affected in all mutant
365 mouse models, the superficial plexus angiogenesis (P0-P8) was largely unperturbed. This is likely because
366 the superficial plexus is fully formed by P8, before the onset of glutamatergic neuronal activity in the mouse
367 retina. This developmental time course can also explain why treatment with 2-amino-4-phosphonobutyrate,
368 a compound that blocks glutamatergic wave, from P3- P7 did not affect retinal angiogenesis in a previous
369 study (Weiner et al., 2019), because the treatment was performed before the onset of glutamatergic wave in
370 the developing mouse retina. Similarly, we found that the transcellular, but not paracellular BRB, was also
371 not affected in the *Vglut1*$^{-/-}$ retina. This is consistent with previous studies showing that transcellular BRB
372 in the mouse retina is fully mature by P10 (Chow and Gu, 2015), whereas paracellular BRB does not fully
373 mature until P18 (Mazzoni et al., 2017). Thus, it is conceivable that glutamatergic neuronal activity kicks
374 in too late to affect the maturation of the transcellular BRB, but has enough time to influence the maturation
375 of the paracellular BRB.
376
377 Interestingly, *Vglut1*$^{-/-}$ retina lacking glutamatergic neuronal activity shows persistent cholinergic
378 wave beyond P10 (Blankenship et al., 2009). Since deficits in the deep plexus angiogenesis and paracellular
379 BRB integrity persist in the *Vglut1*$^{-/-}$ retina throughout P14, these data suggest that the cholinergic wave is
380 not sufficient to promote deep plexus angiogenesis and paracellular BRB maturation. In contrast,
381 paracellular BRB is precociously mature in the *Chrnb2*$^{-/-}$ retina where cholinergic wave is abolished and
382 glutamatergic wave begins earlier (P8) than usual (Bansal et al., 2000). Overall these data indicate that
383 glutamatergic neuronal activity, but not the spontaneous cholinergic activity, is the primary driver to
384 promote paracellular BRB maturation. We were not able to extend our studies beyond P14 in *Vglut1*$^{-/-}$ mice
385 as the pups die around P15 (Fremeau et al., 2004). Notably, the vascular phenotypes, albeit opposite, were

386 more severe in the *Vglut1*$^{-/-}$ retina compared to the *Gnat1*$^{-/-}$ retina. This is likely because glutamate release
387 is abolished from both bipolar cells and photoreceptors (rods and cones) in the *Vglut1*$^{-/-}$ retina (Blankenship
388 et al., 2009). In contrast, only depolarized rod photoreceptors release excess glutamate in the *Gnat1*$^{-/-}$ retina
389 (Calvert et al., 2000; Schroeder et al., 2018). This may likely explain why the vascular phenotypes are less
390 prominent in the P10 *Gnat1*$^{-/-}$ retina, and possibly why the angiogenic phenotype (but not BRB phenotype)
391 in the *Gnat1*$^{-/-}$ retina normalizes to wild-type levels by P14.
392
393 How does extracellular glutamate trigger angiogenesis and BRB maturation in the developing
394 retina? It is possible that the vascular phenotypes in *Vglut1*$^{-/-}$ and *Gnat1*$^{-/-}$ retinas could be due to alterations
395 in either neuronal numbers which have been shown to affect retinal angiogenesis by changing the level of
396 available pro-angiogenic factor VEGF-A (Okabe et al., 2014). However, we did not observe any significant
397 differences in neuronal numbers between WT, *Vglut1*$^{-/-}$ and *Gnat1*$^{-/-}$ retinas, with the exception of a slight
398 decrease in amacrine cells in the *Vglut1*$^{-/-}$ retina. These data suggest that angiogenesis and BRB phenotypes
399 in *Vglut1*$^{-/-}$ and *Gnat1*$^{-/-}$ retinas are not caused by alterations in neuronal numbers. Metabolic demand of
400 retinal neurons also modulates angiogenesis (Joyal et al., 2016; Sapieha et al., 2008; Usui et al., 2015).
401 However, the expression levels of HK2 and PKM2, two key glycolytic enzymes that are readouts of
402 photoreceptor cell metabolism (Cheng et al., 2020), were unaffected in both P10 *Vglut1*$^{-/-}$ and *Gnat1*$^{-/-}$
403 retinas compared to the WT, in spite of the prominent vascular phenotypes in these mutant retinas at this
404 developmental stage. These data suggest that angiogenesis and BRB maturation abnormalities seen in
405 retinas with altered extracellular levels of glutamate are not due to alterations in neuronal numbers and
406 neuronal metabolic demand.
407
408 Our data demonstrate that Norrin mRNA expression and endothelial Norrin/β-catenin activity are
409 downregulated in *Vglut1*$^{-/-}$ retinas, and upregulated in *Gnat1*$^{-/-}$ retinas between P10-P14, and therefore are
410 likely regulated by the extracellular glutamate concentration. Consistent with these findings our scRNA-

411 seq analyses showed that expression levels of effectors of Norrin/β-catenin pathway [*Ctnnb1* and *Lef1*] are
412 downregulated in *Vglut1*$^{-/-}$ retinal ECs. However, Norrin mRNA is expressed in the retina before P10 (Ye
413 et al., 2009), and perturbation of Norrin/β-catenin signaling delays superficial plexus angiogenesis as early
414 as P5 (Wang et al., 2012; Ye et al., 2009), well before the onset of glutamatergic neuronal activity.
415 Therefore, early (P5-P8) Norrin mRNA expression in the retina, which is critical for superficial plexus
416 angiogenesis, is likely regulated by a glutamate-independent mechanism (Macosko et al., 2015). Our data
417 in conjunction with a previous study (Macosko et al., 2015) also suggest that Norrin mRNA is expressed
418 by several cell types in the developing retina including Müller glia as well as INL neurons (horizontal cells
419 and subsets of amacrine and bipolar cells). Further studies will elucidate the relative contribution of Müller
420 glia- or INL neurons-derived Norrin for the deep plexus angiogenesis and paracellular BRB maturation in
421 response to extracellular glutamate. Importantly, pharmacological activation of endothelial Norrin/β-
422 catenin signaling was sufficient to rescue both deep plexus angiogenesis and paracellular BRB integrity in
423 the *Vglut1*$^{-/-}$ retina, consistent with the idea that Wnt/β-catenin signaling functions downstream of
424 extracellular glutamate to promote deep plexus angiogenesis and barriergenesis. Our scRNA-seq data also
425 show a slight downregulation of *Unc5b* in *Vglut1*$^{-/-}$ retinal ECs. Unc5b has been shown to modulate Wnt/β-
426 catenin signaling in CNS ECs (Boye et al., 2022), suggesting the possibility that the cross-talk between
427 these two pathways may be affected in *Vglut1*$^{-/-}$ retinal ECs. Interestingly, none of the downstream targets
428 of VEGF-A signaling was affected in *Vglut1*$^{-/-}$ retinal ECs at the transcriptome level. Thus, VEGF-A
429 signaling pathway does not appear to be regulated by glutamate release in the developing retina.
430
431 Taken together our data suggest a new mechanism by which glutamatergic neuronal activity regulate
432 retinal angiogenesis and BRB maturation in the developing retina **(Figure 8)**. We propose that extracellular
433 glutamate, released either during spontaneous glutamatergic wave or due to light-dependent glutamatergic
434 synaptic activity of photoreceptors from P8 onwards, signals to Müller glia and INL neurons. Glutamate
435 signaling induces Norrin mRNA and protein expression and secretion by Müller glia and INL neurons.

436 Norrin, in turn, activates endothelial Norrin/β-catenin signaling in ECs which promotes angiogenesis in the
437 deep plexus and paracellular BRB maturation in both superficial and deep plexuses of the retina (**Figure**
438 **8**). Our genetic data in *Vglut1*$^{-/-}$ (no glutamate release into the synaptic cleft), *Gnat1*$^{-/-}$ (excess glutamate
439 release into the synaptic cleft) and *Chrnb2*$^{-/-}$ (early onset of glutamatergic wave), and the pharmacological
440 rescue of *Vglut1*$^{-/-}$ phenotypes by activation of the endothelial Wnt/β-catenin signaling are consistent with
441 the proposed model that extracellular glutamate levels control angiogenesis and barriergenesis. Although,
442 the exact mechanism of how glutamate mediates these effects are not fully clear, our single cell RNAseq
443 data together with the published datasets (Macosko et al., 2015) suggest that glutamate cannot act directly
444 on ECs as they do not express either ionotropic or metabotropic glutamate receptor subunits or glutamate
445 transporters. The published transcriptional data of the glutamate receptor and transporter expression
446 (Macosko et al., 2015) and our analysis of the response of the INL cells (neurons and Müller glia) to
447 extracellular glutamate (i.e, changes in GS, GLAST, GLT-1 protein levels) in the *Vglut1*$^{-/-}$ and *Gnat1*$^{-/-}$
448 retinas, suggest that glutamate could directly act on Müller glia and INL neurons to induce *Norrin* mRNA
449 expression. These cells express subsets of ionotropic or metabotropic glutamate receptors and glutamate
450 transporters that make them exquisite sensors of extracellular glutamate levels. In addition, Norrin mRNA
451 is predominantly expressed by the INL cells during vascular development and maturation. Future studies
452 will address in more detail the molecular mechanisms by which glutamate affects Norrin expression by the
453 INL cells. Our findings, not only extend our understanding of the molecular mechanisms by which vascular
454 development and homeostasis occurs in the CNS [reviewed in (Biswas et al., 2020)] including the role that
455 neuronal activity plays in these processes both in the cortex (Lacoste et al., 2014) and retina (Nguyen et al.,
456 2019; Rao et al., 2013; Weiner et al., 2019), but also have important implication to identify potential
457 interventions to treat CNS neurovascular pathologies, including those in the retina such as diabetic
458 retinopathy, or age-related macular degeneration.
459
460

461 **ACKNOWLEDGEMENTS**

462 S.B., S.S., and D.A. are supported by grants from the National Eye Institute (R01EY033994 and
463 K99EY033909), National Heart Lung and Blood Institute (R61HL159949), National Institute of Aging
464 (RF1AG078352), National Institute of Neurological Disorders and Stroke (R21 NS130265), the National
465 Multiple Sclerosis Society (RG-1901-33218) and in part by a gift donation. W.J.B. and G.B. are supported
466 by grants from the National Eye Institute (R01 EY033994-01, R01 EY012676-17, and R21 EY034696) and
467 in part by funds from an unrestricted grant from Research to Prevent Blindness to the Department of
468 Ophthalmology and Visual Sciences, Upstate Medical University.

469

470 **AUTHOR CONTRIBUTIONS**

471 Conceptualization: S.B., W.J.B., D.A.; Methodology: S.B., D.A., G.B.; Software: S.S.; Validation: S.B.,
472 G.B; Formal analysis: S.B., S.S., G.B., P.A.; Investigation: S.B., S.S., G.B.; Resources: W.J.B., D.A.; Data
473 curation: S.B., S.S., G.B.; Writing - original draft: S.B., D.A.; Writing - review & editing: S.B., S.S., W.J.B.,
474 D.A.; Visualization: S.B.; Supervision: D.A., Project administration: D.A., Funding acquisition: W.J.B.,
475 D.A.

476

477 **DECLARATION OF INTEREST**

478 The authors declare no competing or financial interests.

STAR ★ METHODS

Detailed methods are provided in the online version of this paper and include the following:

KEY RESOURCES TABLE

RESOURCE AVAILABILITY

- Lead contact
- Materials availability
- Data and code availability

EXPERIMENTAL MODEL AND SUBJECT DETAILS

- Mice

METHOD DETAILS

- Immunohistochemistry
- Western blot
- Antibodies
- *In situ* hybridization
- Barrier permeability assays
- Retinal endothelial cell isolation
- Single-cell RNA-sequencing analysis
- BIO and MeBIO treatment

QUANTIFICATION AND STATISTICAL ANALYSIS

- Image quantification
- Statistical analysis

STAR ★ METHODS

KEY RESOURCES TABLE

Reagent or resource	Source	Identifier
Primary antibodies		
Rat monoclonal anti-CD31	BD Biosciences	Cat #553370, RRID:AB_394816
FITC rat monoclonal anti-mouse CD31	BD Pharmingen	Cat #553372, RRID:AB_394818
APC rat monoclonal anti-mouse CD31	BD Pharmingen	Cat #551262, RRID:AB_398497
Rabbit monoclonal anti-Ki67	Abcam	Cat #ab16667, RRID:AB_302459
Rabbit monoclonal anti-Cleaved Caspase-3	Cell Signaling Technology	Cat #9664S, RRID:AB_2070042
Goat polyclonal anti-DLL4	R & D Systems	Cat #AF1389, RRID:AB_354770
Rabbit polyclonal anti-Claudin-5	ThermoFisher Scientific	Cat #34-1600, RRID:AB_2533157
Mouse monoclonal anti-ZO-1	ThermoFisher Scientific	Cat #33-9100, RRID:AB_2533147
Rabbit polyclonal anti-SOX9	Millipore Sigma	Cat #ABE571, Lot #2535307
Mouse monoclonal anti-Glutamine synthetase	Millipore Sigma	Cat #MAB302, RRID:AB_2110656
Rabbit monoclonal anti-EAAT1 (GLAST)	Abcam	Cat #ab181036, RRID:AB_2885103

Rabbit polyclonal anti-EAAT2 (GLT-1)	Abcam	Cat #ab41621, RRID:AB_941782
Rabbit polyclonal anti-GFAP	Millipore Sigma	Cat #AB5804, RRID:AB_2109645
Rat monoclonal anti-CD140a (PDGFRα)	BD Biosciences	Cat #558774, RRID:AB_397117
Rabbit monoclonal anti-LEF1	Cell Signaling Technology	Cat# 2230s, RRID:AB_823558
Goat polyclonal anti-PDGFRβ	R & D Systems	Cat #AF1042, RRID:AB_2162633
Rabbit polyclonal anti-Laminin	Millipore Sigma	Cat #L9393, RRID:AB_477163
Rabbit polyclonal anti-Collagen IV	Abcam	Cat #ab6586, RRID:AB_305584
Rabbit polyclonal anti-Aquaporin-4	Millipore Sigma	Cat #A5971, RRID:AB_258270
Rabbit polyclonal anti-Caveolin-1	Abcam	Cat #ab18199, RRID:AB_444314
Rabbit polyclonal anti-PLVAP	Proteintech	Cat #14452-1-AP, RRID:AB_2166100
Mouse monoclonal anti-NeuN	Millipore Sigma	Cat #MAB377, RRID:AB_2298772
Rabbit polyclonal anti-Calbindin	Millipore Sigma	Cat #AB1778, RRID:AB_2068336

Mouse monoclonal anti-PKCα	Santa Cruz Biotechnology	Cat #sc-8393, RRID:AB_628142
Rabbit monoclonal anti-Hexokinase II	Abcam	Cat #ab209847, RRID:AB_2904621
Rabbit monoclonal anti-Pyruvate kinase M2	Cell Signaling Technology	Cat #4053, RRID:AB_1904096
Mouse monoclonal anti-GAPDH	Proteintech	Cat #60004-1-Ig, RRID:AB_2107436
Chemicals, peptides, and recombinant proteins		
Biocytin-TMR (5-(and-6)-tetramethylrhodamine biocytin)	ThermoFisher Scientific	Cat #T12921
Bovine Serum Albumin (BSA), AlexaFluor 594 conjugate	ThermoFisher Scientific	Cat #A13101
Fluorescein-labeled *Griffonia* (*Bandeiraea*) *Simplicifolia* Lectin I (GSL I, BSL I)	Vector Laboratories	Cat #FL-1101, RRID:AB_2336490
6-BIO ((2*Z*,3*E*)-6-bromoindirubin- 3-acetoxime, BIO-Acetoxime)	Calbiochem	Cat #361551
MeBIO (1-methyl-BIO)	Calbiochem	Cat #361556
Propidium iodide	ThermoFisher Scientific	Cat #P1304MP
CD16/CD32 Fc block	BD Pharmingen	Cat #553141
Experimental Models: Organisms/Strains		

Vglut1$^{+/-}$ (C57/BL6J background)	Gift from Dr. Robert H. Edwards (Fremeau et al., 2004)	N/A
Gnat1$^{+/-}$ (C57/BL6J background)	Gift from Dr. William J. Brunken (Calvert et al., 2000)	N/A
Chrnb2$^{+/-}$ (C57/BL6J background)	Gift from Dr. Marina Picciotto (Bansal et al., 2000)	N/A
Oligonucleotides		
Vglut1-WT forward: 5'CCAAGCAAGGTTAAGCCTAG3'	IDT	N/A
Vglut1-WT reverse: 5'GGTGAATTTGGAAAAGAGC3'	IDT	N/A
Vglut1-KO forward: 5'TCGCAGCGCATCGCCTTCTA3'	IDT	N/A
Vglut1-KO reverse: 5'GCCACACGTTTCTTCTGAGG3'	IDT	N/A
Gnat1-WT forward: 5'GCCATCATCTACGGCAACACT CTGC3'	IDT	N/A
Gnat1-WT reverse: 5'GCCGGCGGAATTGAGCTGGTA 3'	IDT	N/A

Gnat1-KO forward: 5'GCCGGTGAATCCGGGAAGAGC 3'	IDT	N/A
Gnat1-KO reverse: 5'GGGCTGCTAAAGCGCATGCTC 3'	IDT	N/A
Chrnb2-WT forward: *5'*CGGAGCATTTGAACTCTG AGCAGTGGGGTCGC3'	IDT	N/A
Chrnb2-WT reverse: 5'CTCGCTGACACAAGGGCT GCGGAC3'	IDT	N/A
Chrnb2-KO forward: *5'*CACTACGTCTGAACG TCGAAAACCCG3'	IDT	N/A
Chrnb2-KO reverse: 5'CGGGCAAATAATATC GGTGGCCGTGG3'	IDT	N/A
Softwares and algorithms		
ImageJ/Fiji	NIH	https://imagej.net/software/fiji/downloads
Zen microscopy software	ZEISS	https://www.zeiss.com/microscopy/en/products/software/zeiss-zen.html#packages

Seurat	Seurat	https://satijalab.org/seurat/
Tidyverse	Tidyverse	https://www.tidyverse.org
DAVID	DAVID bioinformatics resources	https://david.ncifcrf.gov
Prism 9	GraphPad	https://www.graphpad.com/scientific-software/prism/
Other		
RNA *in situ* probe for mouse *Ndp* (Norrin)	(Mazzoni et al., 2017)	N/A
RNA *in situ* probe for full-length mouse *Apcdd1*	(Mazzoni et al., 2017)	N/A
C57B6 wild-type P14 retina by drop-seq (single-cell RNA-sequencing database)	(Macosko et al., 2015)	https://singlecell.broadinstitute.org/single_cell/study/SCP301/c57b6-wild-type-p14-retina-by-drop-seq

RESOURCE AVAILABILITY

Lead contact

Further information and requests for resources and reagents should be directed to the lead contact, Dritan Agalliu (da191@cumc.columbia.edu).

Materials availability

This study did not generate new unique reagents.

513 **Data and code availability**

514 All data are available in the manuscript and the supplementary information. The codes used in this study
515 have been previously published and are freely available (see Key Resources Table). Any additional
516 information required to reanalyze the data reported in this study will be available upon request.

517

518 **EXPERIMENTAL MODEL AND SUBJECT DETAILS**

519 **Mice**

520 All animal usage and protocols were approved by the Institutional Animal Care and Use Committee
521 (IACUC) at Columbia University Irving Medical Center. Experimental procedures were optimized to
522 minimize animal stress and the number of animals used for experiments. Mice were maintained on 12
523 light/12 dark cycle. Both sexes (males and females) were used for experiments and analyses. All mice were
524 maintained in C57/BL6J background. The *in vivo* BRB permeability assays were performed either at P10
525 or P14. Generation of *Vglut1*$^{-/-}$ mice was described before (Fremeau et al., 2004). These mice were bred as
526 heterozygous and gave birth in Mendelian ratios. Age-matched littermate WT and *Vglut1*$^{-/-}$ mice were used
527 for experiments (*Vglut1*$^{-/-}$ mice die around P15). Generation of *Gnat1*$^{-/-}$ mice was described before (Calvert
528 et al., 2000). These mice were bred as heterozygous and gave birth in Mendelian ratios. Age-matched
529 littermate WT and *Gnat1*$^{-/-}$ mice were used for experiments. Note that *Gnat1*$^{-/-}$ mice a viable and fertile.
530 Generation of *Chrnb2*$^{-/-}$ mice was described before (Bansal et al., 2000). These mice were bred as *Chrnb2*$^{+/-}$
531 and gave birth in Mendelian ratios. Age-matched littermate WT and *Chrnb2*$^{-/-}$ mice were used for
532 experiments. Note that *Chrnb2*$^{-/-}$ mice a viable and fertile.

533

534 **METHOD DETAILS**

535 **Immunofluorescence**

536 Unless otherwise specified, isolated tissues (retina, brain and liver) were fixed in 4% PFA for 2
537 hours for immunostaining. The exceptions were retinal flat-mount staining for Laminin, in which cases

538 retinas were fixed for 10 minutes in 2% PFA. For retinal flat-mounts, tissues were washed with 1X PBS
539 following PFA fixation and blocked overnight in blocking buffer (5% goat or donkey serum, 0.3% Triton
540 X-100 in 1× PBS) at 4°C. Samples were then incubated with primary antibodies in antibody-diluting
541 solution (5% goat or donkey serum; 0.01% Triton X-100 in 1X PBS) for 48h at 4°C, washed, and incubated
542 with secondary antibodies for 24 h. For radial section staining, samples were washed in 1 × PBS,
543 cryoprotected in 30% sucrose overnight, embedded in optimal cutting temperature compound (Tissue-Tek;
544 Torrance, CA, USA), and sectioned at a thickness of 12 μm. Tissue sections were blocked for 2 h at room
545 temperature followed by primary antibody incubation overnight at 4°C. Following 1X PBS washes, sections
546 were incubated with secondary antibodies for 4 h at room temperature. Samples were imaged in room
547 temperature using a Zeiss LSM700 confocal microscope [ZEISS 20X air (Objective Plan-Apochromat
548 20x/0.8 M27; numerical aperture: 0.8) or 40X water (Objective C-Apochromat 40x/1.2 W autocorr M27;
549 numerical aperture: 1.2) objectives; ZEN image acquisition software] and analyzed using Fiji software.
550

551 **Western blotting**

552 Retinas were collected from mice after perfusion with PBS. Six retinas from three mice were
553 combined for each sample. Collected tissue was homogenized in lysis buffer containing protease and
554 phosphatase inhibitors using a Dounce homogenizer followed by sonication. Protein concentration was
555 assayed by BCA (Bio-Rad) and resolved on SDS-PAGE. Protein levels in P10 retinas were measured by
556 fluorescent western blot analysis [4-15% or 7.5% Mini-PROTEAN TGX gels (Bio-Rad)] and quantitation
557 was performed using the LICOR system, as previously described. Fluorescent quantification of protein
558 levels was performed using the Odyssey SA infrared imaging system. Values are displayed as protein levels
559 corrected with GAPDH (loading control) and normalized to the WT values.
560

561 **Antibodies**

562 Primary antibodies used were rat anti-CD31 (BD Biosciences, Cat #553370, 1:250), rabbit anti-Ki67
563 (Abcam, Cat #ab16667, 1:500), rabbit anti-cleaved Caspase-3 (Cell Signaling Technology, Cat #9664S,
564 1:500), Goat anti-DLL4 (R & D Systems, Cat #AF1389, 1:200), rabbit anti-Claudin-5 (ThermoFisher
565 Scientific, Cat #34-1600, 1:500), rabbit anti-SOX9 (Millipore Sigma, Cat #ABE571, 1:500), mouse anti-
566 Glutamine Synthetase (Millipore Sigma, Cat #MAB302, 1:500), rabbit anti-EAAT1 (Abcam, Cat
567 #ab181036, 1:250), rabbit anti-EAAT2 (Abcam, Cat #ab41621, 1:250), rabbit anti-GFAP (Millipore Sigma,
568 Cat #AB5804, 1:500), rat anti-CD140a (BD Biosciences, Cat #558774, 1:100), rabbit anti-LEF1 (Cell
569 Signaling Technology, Cat #2230s, 1:100), goat anti-PDGFRβ (R & D Systems, Cat #AF1042, 1:250),
570 rabbit anti-Laminin (Millipore Sigma, Cat #L9393, 1:500), rabbit anti-Aquaporin-4 (Millipore Sigma, Cat
571 #A5971, 1:250), rabbit anti-Caveolin-1 (Abcam, Cat #ab18199, 1:500), rabbit anti-PLVAP (Proteintech,
572 Cat #14452-1-AP, 1:250), mouse anti-NeuN (Millipore Sigma, Cat #MAB377, 1:500), rabbit anti-
573 Calbindin (Millipore Sigma, Cat #AB1778, 1:250), mouse anti-PKCα (Santa Cruz Biotechnology, Cat #sc-
574 8393, 1:1000), rabbit anti-Hexokinase II (Abcam, Cat #ab209847, 1:1000), rabbit anti-Pyruvate Kinase M2
575 (Cell Signaling Technology, Cat #4053, 1:1000), mouse anti-GAPDH (Proteintech, Cat #60004-1-Ig,
576 1:50000), FITC rat anti-mouse CD31 (BD Pharmingen, Cat #553372, 1:200), and APC rat anti-mouse
577 CD31 (BD Pharmingen, Cat #551262, 1:200). Secondary antibodies used were: goat anti-rat Alexa Fluor
578 594 (A11007), goat anti-rabbit Alexa Fluor 594 (A11012), goat anti-rat Alexa Fluor 488 (A11006), goat
579 anti-rabbit Alexa Fluor 488 (A11034), donkey anti-rat Alexa Fluor 594 (A21209), donkey anti-rabbit Alexa
580 Fluor 594 (A32754), donkey anti-rat Alexa Fluor 488 (A21208), donkey anti-rabbit Alexa Fluor 488
581 (A21206), donkey anti-rat Alexa Fluor 647 (A48272), donkey anti-rabbit Alexa Fluor 647 (A32795),
582 donkey anti-goat Alexa Fluor 594 (A32758) and donkey anti-goat Alexa Fluor 488 (A11055) (all 1:250;
583 ThermoFisher Scientific). IRDyes 680 and 800 (1:20000; LI-COR) were used as secondary antibodies for
584 Western blot.
585
586 ***In situ* hybridization**

587 Both alkaline phosphatase and fluorescent *in situ* hybridization of retinal sections using antisense mRNA
588 probe for full-length mouse *Apcdd1* and *Ndp* (Norrin) were performed as described before (Mazzoni et al.,
589 2017). The samples were imaged using either a ZEISS Axio Imager (alkaline phosphatase) or a ZEISS
590 LSM700 confocal (fluorescent) microscope and analyzed using Fiji software.
591
592 **Barrier permeability assays**
593 Mice were anesthetized using isoflurane and injected with either 1% Biocytin-5(and-6-)-
594 Tetramethylrhodamine (biocytin-TMR: ThermoFisher Scientific, Cat #T12921) or 1% Bovine Serum
595 Albumin (BSA) - AlexaFluor 594 conjugate (albumin-Alexa594: ThermoFisher Scientific, Cat #A13101).
596 After 40 minutes in circulation, mice were re-anesthetized and perfused with 1X PBS via the cardiac route.
597 Retinas and livers were isolated and fixed in 4% PFA for 2 hours prior to immunostaining with FITC-
598 conjugated Lectin. Since blood vessels in the liver do not have a barrier, Biocytin-TMR or Albumin-594
599 fluorescence levels in the livers of corresponding animals were used as internal controls for measurement
600 of biocytin-TMR and albumin-Alexa594 fluorescence levels in the retinas as described (Biswas et al., 2022;
601 Mazzoni et al., 2017).
602
603 **Retinal endothelial cell isolation**
604 P10 WT and *Vglut1*$^{-/-}$ as well as P14 WT mice were anesthetized using isoflurane and perfused for 4 minutes
605 with ice-cold sterile 1X PBS. The eyes were enucleated and retinas were dissected in Earl's balanced salt
606 solution (EBSS). Retinas were dissociated in a single-cell suspension using a published protocol
607 (Vanlandewijck et al., 2018). Once the retinas were dissociated into single cells, it was resuspended in 200
608 ml of CD16/CD32 Fc block (BD Pharmingen, Cat #553141, 1:200 in FACS buffer) and incubated at
609 room temperature for 15 minutes. The samples were washed with 2 ml of FACS buffer, with 100 ml kept
610 aside for use as unstained and fluorescence minus one (FMO) controls. The cells were then resuspended in
611 200 ml of anti-mouse CD31 [either FITC rat anti-mouse CD31 (BD Pharmingen, Cat #553372, 1:200) or

612 and APC rat anti-mouse CD31 (BD Pharmingen, Cat #551262), 1:200 in FACS buffer)] antibody to label
613 ECs, covered in aluminum foil and incubated on ice for 60 mins. Following antibody labeling, the samples
614 were washed twice with 2 ml of FACS buffer and resuspended in 400 ml of propidium
615 iodide (Thermofisher, Cat. #P1304MP; 1/10,000 in FACS buffer). Gates for the surface stain were set using
616 the unstained and FMO controls, and either CD31-APC^{+} or CD31-FITC^{+} ECs were sorted out using the
617 BD FACSAria Flow Cytometer (Columbia Stem Cell Initiative Flow Cytometry Core) for single-cell RNA-
618 sequencing.
619

620 **Single-cell RNA-sequencing (scRNA-seq) analysis**

621 Total of 1104 ECs for P10 WT retinas and 1046 ECs for P10 *Vglut1*$^{-/-}$ retinas were analyzed for differential
622 gene expression analyses (**Table S1**). The 10x Genomics Chromium platform (Yuan et al., 2018; Yuan and
623 Sims, 2016) was used to generate low-depth data (~2000 genes/cell), and was processed using the Cell
624 Ranger analysis pipeline to align reads and generate feature-barcode matrices. The Seurat R package (Hao
625 et al., 2021) was implemented to read the output of the Cell Ranger pipeline and merge cells from all the
626 samples (WT and mutant) into a single R object. The standard pre-processing workflow for scRNAseq data
627 was carried out in Seurat, which consisted of the selection and filtration of cells based on quality control
628 metrics (e.g., number of unique genes detected in each cell > 200, total number of molecules detected within
629 a cell > 1,000 and < 50,000, percentage of reads within a cell that map to the mitochondrial genome < 20,
630 etc.), data normalization and scaling, and the detection of highly variable features. Next, linear
631 dimensionality reduction (PCA) was performed on the scaled data using the previously determined highly
632 variable features, an alternative heuristic method ('Elbow plot') was implemented to determine the
633 'dimensionality' of the dataset, and cells were clustered by applying the weighted shared nearest-neighbor
634 graph-based clustering method using the first 20 PCs (Menon, 2018). Lastly, the 20 PCA dimensions were
635 further reduced into two-dimensional space using the non-linear dimensional reduction technique, uniform
636 manifold approximation and projection for dimension reduction (UMAP), to visualize and explore the

637 scRNA-seq dataset and each of its unique EC clusters. From the gene signatures that are uniquely present
638 in mutant ECs compared to WT ECs, and validated by fluorescent in situ hybridization and/or
639 immunofluorescence. Gene ontology (GO) enrichment analysis was performed using DAVID
640 bioinformatics database to elucidate significantly up- and downregulated pathways in mutant ECs.
641

642 **BIO and MeBIO treatment**

643 The *in vivo* injections of 6-BIO ((2*Z*,3*E*)-6-bromoindirubin- 3-acetoxime, BIO-Acetoxime; Calbiochem,
644 Cat #361551) and control MeBIO (1-methyl-BIO; Calbiochem, Cat #361556) were performed as previously
645 published (Corada et al., 2019). Pups were anesthetized with 1% isoflurane. Intraperitoneal injections of
646 BIO and MeBIO were performed at a concentration of 5 mg/kg/day in sterile PBS from P6 to P8. Injected
647 pups were re-anesthetized and perfused with 1X PBS to harvest tissues for analyses at P10.
648

649 **QUANTIFICATION AND STATISTICAL ANALYSIS**

650 **Image quantification**

651 For retinal flat-mounts, each measurement was made in at least 3 quadrants per sample. The measurements
652 were done separately in the central (near the optic nerve-head) and peripheral (near the edge) retina. For
653 sections, at least three sections were imaged per sample. In each case, multiple representative images were
654 acquired and averaged. To measure vascular area and branch point density, area positive for CD31 or Lectin
655 was measured from each image in Fiji software (National Institutes of Health) using signal masking. Branch
656 point numbers were normalized to unit area (1 mm^2). To measure number of proliferative or apoptotic ECs,
657 the number of $Ki67^+$ or cleaved Caspase-3^+ ECs, respectively, were normalized to unit $CD31^+$ vascular area
658 (1 mm^2). The area of Biocytin-TMR leakage was done separately in the central and peripheral retina. The
659 intensity of biocytin-TMR and albumin-Alexa594 outside of retinal vessels was measured as described
660 (Mazzoni et al., 2017). Biocytin-TMR and albumin-Alexa594 signal intensities in the retina and cerebella
661 were normalized to those of livers. For vascular area positive for Claudin-5 and Caveolin-1, area positive

662 for Lectin was selected from each image in Fiji software using signal masking, followed by measuring the
663 percentage of Lectin$^+$/Claudin-5$^+$ or Lectin$^+$/Caveolin-1$^+$ in corresponding images. To measure the number
664 of ganglion (NeuN$^+$), amacrine, horizontal (Calbindin$^+$) and bipolar cells (PKCα^+), the number of cells were
665 normalized to the length of either ganglion cell layer (GCL; for ganglion cells) or inner nuclear layer (INL;
666 for amacrine, horizontal and bipolar cells). To measure the number of photoreceptors, the thickness of the
667 outer nuclear layer (ONL) was quantified as a function of photoreceptor number. To measure the number
668 of Müller glia, the number of Sox9$^+$ cells were normalized to the length of INL. To measure the relative
669 expression of GS and GLAST, the M.F.I were calculated for each field and data was presented as values
670 normalized to the number of Sox9$^+$ Müller glia. To measure *Ndp* expression, mean fluorescence intensity
671 (M.F.I) of *Ndp* in the INL was calculated with histogram analysis in Fiji software and normalized to the
672 WT values. For Lef1$^+$ EC quantification, the number of Lef1$^+$ ECs was normalized to unit CD31$^+$ or Lectin$^+$
673 vascular area (1 mm^2). For western blots, values are displayed as target protein levels corrected with
674 GAPDH (loading control) and normalized to the WT values using Odyssey SA infrared imaging system.
675

676 **Statistical analysis**

677 Retinas from 3-5 different animals (for *in vivo* experiments) were used for statistical analysis. For western
678 blots, retinas from 3 animals/genotype were combined into one sample, and 4 samples/genotype was used
679 for quantification. To test for statistical significance of any differences, unpaired Student's *t* test was
680 performed using GraphPad Prism. A value of $P < 0.05$ was considered statistically significant. For scRNA-
681 seq analysis, we considered transcripts with adjusted p value < 0.05, and >1.2-fold ($\log_2$fc > 0.25 and $\log_2$fc
682 < -0.25) difference in expression as significant. For GO analysis, Gene sets with false discovery rate (FDR)
683 < 0.01 were considered significant.

684 **REFERENCES**

685

686 Abcouwer, S.F., and Gardner, T.W. (2014). Diabetic retinopathy: loss of neuroretinal adaptation to the
687 diabetic metabolic environment. Ann N Y Acad Sci *1311*, 174-190.

688 Bansal, A., Singer, J.H., Hwang, B.J., Xu, W., Beaudet, A., and Feller, M.B. (2000). Mice lacking specific
689 nicotinic acetylcholine receptor subunits exhibit dramatically altered spontaneous activity patterns and
690 reveal a limited role for retinal waves in forming ON and OFF circuits in the inner retina. J Neurosci *20*,
691 7672-7681.

692 Biswas, S., Cottarelli, A., and Agalliu, D. (2020). Neuronal and glial regulation of CNS angiogenesis and
693 barriergenesis. Development *147*.

694 Biswas, S., Shahriar, S., Giangreco, N.P., Arvanitis, P., Winkler, M., Tatonetti, N.P., Brunken, W.J.,
695 Cutforth, T., and Agalliu, D. (2022). Mural Wnt/beta-catenin signaling regulates Lama2 expression to
696 promote neurovascular unit maturation. Development *149*.

697 Blankenship, A.G., Ford, K.J., Johnson, J., Seal, R.P., Edwards, R.H., Copenhagen, D.R., and Feller, M.B.
698 (2009). Synaptic and extrasynaptic factors governing glutamatergic retinal waves. Neuron *62*, 230-241.

699 Boccuni, I., and Fairless, R. (2022). Retinal Glutamate Neurotransmission: From Physiology to
700 Pathophysiological Mechanisms of Retinal Ganglion Cell Degeneration. Life (Basel) *12*.

701 Bonezzi, P.J., Stabio, M.E., and Renna, J.M. (2018). The Development of Mid-Wavelength
702 Photoresponsivity in the Mouse Retina. Curr Eye Res *43*, 666-673.

703 Bosma, E.K., van Noorden, C.J.F., Schlingemann, R.O., and Klaassen, I. (2018). The role of plasmalemma
704 vesicle-associated protein in pathological breakdown of blood-brain and blood-retinal barriers: potential
705 novel therapeutic target for cerebral edema and diabetic macular edema. Fluids Barriers CNS *15*, 24.

706 Boye, K., Geraldo, L.H., Furtado, J., Pibouin-Fragner, L., Poulet, M., Kim, D., Nelson, B., Xu, Y., Jacob,
707 L., Maissa, N.*, et al.* (2022). Endothelial Unc5B controls blood-brain barrier integrity. Nat Commun *13*,
708 1169.

709 Buckingham, B.P., Inman, D.M., Lambert, W., Oglesby, E., Calkins, D.J., Steele, M.R., Vetter, M.L.,
710 Marsh-Armstrong, N., and Horner, P.J. (2008). Progressive ganglion cell degeneration precedes neuronal
711 loss in a mouse model of glaucoma. J Neurosci *28*, 2735-2744.
712 Calvert, P.D., Krasnoperova, N.V., Lyubarsky, A.L., Isayama, T., Nicolo, M., Kosaras, B., Wong, G.,
713 Gannon, K.S., Margolskee, R.F., Sidman, R.L.*, et al.* (2000). Phototransduction in transgenic mice after
714 targeted deletion of the rod transducin alpha -subunit. Proc Natl Acad Sci U S A *97*, 13913-13918.
715 Chan-Ling, T., and Stone, J. (1992). Degeneration of astrocytes in feline retinopathy of prematurity causes
716 failure of the blood-retinal barrier. Invest Ophthalmol Vis Sci *33*, 2148-2159.
717 Cheng, S.Y., Cipi, J., Ma, S., Hafler, B.P., Kanadia, R.N., Brush, R.S., Agbaga, M.P., and Punzo, C. (2020).
718 Altered photoreceptor metabolism in mouse causes late stage age-related macular degeneration-like
719 pathologies. Proc Natl Acad Sci U S A *117*, 13094-13104.
720 Chow, B.W., and Gu, C. (2015). The molecular constituents of the blood-brain barrier. Trends Neurosci *38*,
721 598-608.
722 Chow, B.W., and Gu, C. (2017). Gradual Suppression of Transcytosis Governs Functional Blood-Retinal
723 Barrier Formation. Neuron *93*, 1325-1333 e1323.
724 Corada, M., Orsenigo, F., Bhat, G.P., Conze, L.L., Breviario, F., Cunha, S.I., Claesson-Welsh, L.,
725 Beznoussenko, G.V., Mironov, A.A., Bacigaluppi, M.*, et al.* (2019). Fine-Tuning of Sox17 and Canonical
726 Wnt Coordinates the Permeability Properties of the Blood-Brain Barrier. Circ Res *124*, 511-525.
727 Feit-Leichman, R.A., Kinouchi, R., Takeda, M., Fan, Z., Mohr, S., Kern, T.S., and Chen, D.F. (2005).
728 Vascular damage in a mouse model of diabetic retinopathy: relation to neuronal and glial changes. Invest
729 Ophthalmol Vis Sci *46*, 4281-4287.
730 Feller, M.B., Wellis, D.P., Stellwagen, D., Werblin, F.S., and Shatz, C.J. (1996). Requirement for
731 cholinergic synaptic transmission in the propagation of spontaneous retinal waves. Science *272*, 1182-1187.

732 Fremeau, R.T., Jr., Kam, K., Qureshi, T., Johnson, J., Copenhagen, D.R., Storm-Mathisen, J., Chaudhry,
733 F.A., Nicoll, R.A., and Edwards, R.H. (2004). Vesicular glutamate transporters 1 and 2 target to functionally
734 distinct synaptic release sites. Science *304*, 1815-1819.
735 Gu, X., Reagan, A., Yen, A., Bhatti, F., Cohen, A.W., and Elliott, M.H. (2014). Spatial and temporal
736 localization of caveolin-1 protein in the developing retina. Adv Exp Med Biol *801*, 15-21.
737 Hajdu, R.I., Laurik, L.K., Szabo, K., Dekany, B., Almasi, Z., Enzsoly, A., Szabo, A., Radovits, T., Matyas,
738 C., Olah, A.*, et al.* (2019). Detailed Evaluation of Possible Ganglion Cell Loss in the Retina of Zucker
739 Diabetic Fatty (ZDF) Rats. Sci Rep *9*, 10463.
740 Hao, Y., Hao, S., Andersen-Nissen, E., Mauck, W.M., 3rd, Zheng, S., Butler, A., Lee, M.J., Wilk, A.J.,
741 Darby, C., Zager, M.*, et al.* (2021). Integrated analysis of multimodal single-cell data. Cell *184*, 3573-3587
742 e3529.
743 Harada, T., Harada, C., Watanabe, M., Inoue, Y., Sakagawa, T., Nakayama, N., Sasaki, S., Okuyama, S.,
744 Watase, K., Wada, K.*, et al.* (1998). Functions of the two glutamate transporters GLAST and GLT-1 in the
745 retina. Proc Natl Acad Sci U S A *95*, 4663-4666.
746 Hellstrom, M., Phng, L.K., Hofmann, J.J., Wallgard, E., Coultas, L., Lindblom, P., Alva, J., Nilsson, A.K.,
747 Karlsson, L., Gaiano, N.*, et al.* (2007). Dll4 signalling through Notch1 regulates formation of tip cells
748 during angiogenesis. Nature *445*, 776-780.
749 Hippert, C., Graca, A.B., Barber, A.C., West, E.L., Smith, A.J., Ali, R.R., and Pearson, R.A. (2015). Muller
750 glia activation in response to inherited retinal degeneration is highly varied and disease-specific. PLoS One
751 *10*, e0120415.
752 Hupe, M., Li, M.X., Kneitz, S., Davydova, D., Yokota, C., Kele, J., Hot, B., Stenman, J.M., and Gessler,
753 M. (2017). Gene expression profiles of brain endothelial cells during embryonic development at bulk and
754 single-cell levels. Sci Signal *10*.
755 Jones, B.W., Pfeiffer, R.L., Ferrell, W.D., Watt, C.B., Marmor, M., and Marc, R.E. (2016a). Retinal
756 remodeling in human retinitis pigmentosa. Exp Eye Res *150*, 149-165.

757 Jones, B.W., Pfeiffer, R.L., Ferrell, W.D., Watt, C.B., Tucker, J., and Marc, R.E. (2016b). Retinal
758 Remodeling and Metabolic Alterations in Human AMD. Front Cell Neurosci *10*, 103.
759 Joyal, J.S., Sun, Y., Gantner, M.L., Shao, Z., Evans, L.P., Saba, N., Fredrick, T., Burnim, S., Kim, J.S.,
760 Patel, G.*, et al.* (2016). Retinal lipid and glucose metabolism dictates angiogenesis through the lipid sensor
761 Ffar1. Nat Med *22*, 439-445.
762 Junge, H.J., Yang, S., Burton, J.B., Paes, K., Shu, X., French, D.M., Costa, M., Rice, D.S., and Ye, W.
763 (2009). TSPAN12 regulates retinal vascular development by promoting Norrin- but not Wnt-induced
764 FZD4/beta-catenin signaling. Cell *139*, 299-311.
765 Klaassen, I., Van Noorden, C.J., and Schlingemann, R.O. (2013). Molecular basis of the inner blood-retinal
766 barrier and its breakdown in diabetic macular edema and other pathological conditions. Prog Retin Eye Res
767 *34*, 19-48.
768 Lacoste, B., Comin, C.H., Ben-Zvi, A., Kaeser, P.S., Xu, X., Costa Lda, F., and Gu, C. (2014). Sensory-
769 related neural activity regulates the structure of vascular networks in the cerebral cortex. Neuron *83*, 1117-
770 1130.
771 Lee, S.H., Park, Y.S., Paik, S.S., and Kim, I.B. (2021). Differential Response of Muller Cells and Microglia
772 in a Mouse Retinal Detachment Model and Its Implications in Detached and Non-Detached Regions. Cells
773 *10*.
774 Liegl, R., Hellstrom, A., and Smith, L.E. (2016). Retinopathy of prematurity: the need for prevention. Eye
775 Brain *8*, 91-102.
776 Luhmann, U.F., Lin, J., Acar, N., Lammel, S., Feil, S., Grimm, C., Seeliger, M.W., Hammes, H.P., and
777 Berger, W. (2005). Role of the Norrie disease pseudoglioma gene in sprouting angiogenesis during
778 development of the retinal vasculature. Invest Ophthalmol Vis Sci *46*, 3372-3382.
779 Macosko, E.Z., Basu, A., Satija, R., Nemesh, J., Shekhar, K., Goldman, M., Tirosh, I., Bialas, A.R.,
780 Kamitaki, N., Martersteck, E.M.*, et al.* (2015). Highly Parallel Genome-wide Expression Profiling of
781 Individual Cells Using Nanoliter Droplets. Cell *161*, 1202-1214.

782 Mazzoni, J., Smith, J.R., Shahriar, S., Cutforth, T., Ceja, B., and Agalliu, D. (2017). The Wnt Inhibitor
783 Apcdd1 Coordinates Vascular Remodeling and Barrier Maturation of Retinal Blood Vessels. Neuron *96*,
784 1055-1069 e1056.
785 Menon, V. (2018). Clustering single cells: a review of approaches on high-and low-depth single-cell RNA-
786 seq data. Brief Funct Genomics *17*, 240-245.
787 Nguyen, M.T., Vemaraju, S., Nayak, G., Odaka, Y., Buhr, E.D., Alonzo, N., Tran, U., Batie, M., Upton,
788 B.A., Darvas, M.*, et al.* (2019). An opsin 5-dopamine pathway mediates light-dependent vascular
789 development in the eye. Nat Cell Biol *21*, 420-429.
790 Okabe, K., Kobayashi, S., Yamada, T., Kurihara, T., Tai-Nagara, I., Miyamoto, T., Mukouyama, Y.S., Sato,
791 T.N., Suda, T., Ema, M.*, et al.* (2014). Neurons limit angiogenesis by titrating VEGF in retina. Cell *159*,
792 584-596.
793 Okawa, H., Sampath, A.P., Laughlin, S.B., and Fain, G.L. (2008). ATP consumption by mammalian rod
794 photoreceptors in darkness and in light. Curr Biol *18*, 1917-1921.
795 Paes, K.T., Wang, E., Henze, K., Vogel, P., Read, R., Suwanichkul, A., Kirkpatrick, L.L., Potter, D.,
796 Newhouse, M.M., and Rice, D.S. (2011). Frizzled 4 is required for retinal angiogenesis and maintenance of
797 the blood-retina barrier. Invest Ophthalmol Vis Sci *52*, 6452-6461.
798 Pardue, M.T., Barnes, C.S., Kim, M.K., Aung, M.H., Amarnath, R., Olson, D.E., and Thule, P.M. (2014).
799 Rodent Hyperglycemia-Induced Inner Retinal Deficits are Mirrored in Human Diabetes. Transl Vis Sci
800 Technol *3*, 6.
801 Pfeiffer, R.L., Marc, R.E., Kondo, M., Terasaki, H., and Jones, B.W. (2016). Muller cell metabolic chaos
802 during retinal degeneration. Exp Eye Res *150*, 62-70.
803 Poche, R.A., Furuta, Y., Chaboissier, M.C., Schedl, A., and Behringer, R.R. (2008). Sox9 is expressed in
804 mouse multipotent retinal progenitor cells and functions in Muller glial cell development. J Comp Neurol
805 *510*, 237-250.

806 Prokofyeva, E., and Zrenner, E. (2012). Epidemiology of major eye diseases leading to blindness in Europe:
807 a literature review. Ophthalmic Res *47*, 171-188.
808 Rao, S., Chun, C., Fan, J., Kofron, J.M., Yang, M.B., Hegde, R.S., Ferrara, N., Copenhagen, D.R., and
809 Lang, R.A. (2013). A direct and melanopsin-dependent fetal light response regulates mouse eye
810 development. Nature *494*, 243-246.
811 Russo, R., Cavaliere, F., Varano, G.P., Milanese, M., Adornetto, A., Nucci, C., Bonanno, G., Morrone,
812 L.A., Corasaniti, M.T., and Bagetta, G. (2013). Impairment of neuronal glutamate uptake and modulation
813 of the glutamate transporter GLT-1 induced by retinal ischemia. PLoS One *8*, e69250.
814 Sapieha, P., Sirinyan, M., Hamel, D., Zaniolo, K., Joyal, J.S., Cho, J.H., Honore, J.C., Kermorvant-
815 Duchemin, E., Varma, D.R., Tremblay, S.*, et al.* (2008). The succinate receptor GPR91 in neurons has a
816 major role in retinal angiogenesis. Nat Med *14*, 1067-1076.
817 Schroeder, M.M., Harrison, K.R., Jaeckel, E.R., Berger, H.N., Zhao, X., Flannery, M.P., St Pierre, E.C.,
818 Pateqi, N., Jachimska, A., Chervenak, A.P.*, et al.* (2018). The Roles of Rods, Cones, and Melanopsin in
819 Photoresponses of M4 Intrinsically Photosensitive Retinal Ganglion Cells (ipRGCs) and Optokinetic Visual
820 Behavior. Front Cell Neurosci *12*, 203.
821 Schweighofer, B., Testori, J., Sturtzel, C., Sattler, S., Mayer, H., Wagner, O., Bilban, M., and Hofer, E.
822 (2009). The VEGF-induced transcriptional response comprises gene clusters at the crossroad of
823 angiogenesis and inflammation. Thromb Haemost *102*, 544-554.
824 Serjanov, D., Bachay, G., Hunter, D.D., and Brunken, W.J. (2018). Laminin beta2 Chain Regulates Retinal
825 Progenitor Cell Mitotic Spindle Orientation via Dystroglycan. J Neurosci *38*, 5996-6010.
826 Shen, F., Chen, B., Danias, J., Lee, K.C., Lee, H., Su, Y., Podos, S.M., and Mittag, T.W. (2004). Glutamate-
827 induced glutamine synthetase expression in retinal Muller cells after short-term ocular hypertension in the
828 rat. Invest Ophthalmol Vis Sci *45*, 3107-3112.

829 Sherry, D.M., Wang, M.M., Bates, J., and Frishman, L.J. (2003). Expression of vesicular glutamate
830 transporter 1 in the mouse retina reveals temporal ordering in development of rod vs. cone and ON vs. OFF
831 circuits. J Comp Neurol *465*, 480-498.
832 Siemerink, M.J., Klaassen, I., Van Noorden, C.J., and Schlingemann, R.O. (2013). Endothelial tip cells in
833 ocular angiogenesis: potential target for anti-angiogenesis therapy. J Histochem Cytochem *61*, 101-115.
834 Stahl, A., Connor, K.M., Sapieha, P., Chen, J., Dennison, R.J., Krah, N.M., Seaward, M.R., Willett, K.L.,
835 Aderman, C.M., Guerin, K.I.*, et al.* (2010). The mouse retina as an angiogenesis model. Invest Ophthalmol
836 Vis Sci *51*, 2813-2826.
837 Suchting, S., Freitas, C., le Noble, F., Benedito, R., Breant, C., Duarte, A., and Eichmann, A. (2007). The
838 Notch ligand Delta-like 4 negatively regulates endothelial tip cell formation and vessel branching. Proc
839 Natl Acad Sci U S A *104*, 3225-3230.
840 Taylor, S., Srinivasan, B., Wordinger, R.J., and Roque, R.S. (2003). Glutamate stimulates neurotrophin
841 expression in cultured Muller cells. Brain Res Mol Brain Res *111*, 189-197.
842 Tiriac, A., Smith, B.E., and Feller, M.B. (2018). Light Prior to Eye Opening Promotes Retinal Waves and
843 Eye-Specific Segregation. Neuron *100*, 1059-1065 e1054.
844 Umino, Y., and Solessio, E. (2013). Loss of scotopic contrast sensitivity in the optomotor response of
845 diabetic mice. Invest Ophthalmol Vis Sci *54*, 1536-1543.
846 Usui, Y., Westenskow, P.D., Kurihara, T., Aguilar, E., Sakimoto, S., Paris, L.P., Wittgrove, C., Feitelberg,
847 D., Friedlander, M.S., Moreno, S.K.*, et al.* (2015). Neurovascular crosstalk between interneurons and
848 capillaries is required for vision. J Clin Invest *125*, 2335-2346.
849 Vanlandewijck, M., He, L., Mae, M.A., Andrae, J., Ando, K., Del Gaudio, F., Nahar, K., Lebouvier, T.,
850 Lavina, B., Gouveia, L.*, et al.* (2018). A molecular atlas of cell types and zonation in the brain vasculature.
851 Nature *554*, 475-480.
852 Wang, Y., Rattner, A., Zhou, Y., Williams, J., Smallwood, P.M., and Nathans, J. (2012). Norrin/Frizzled4
853 signaling in retinal vascular development and blood brain barrier plasticity. Cell *151*, 1332-1344.

854 Weiner, G.A., Shah, S.H., Angelopoulos, C.M., Bartakova, A.B., Pulido, R.S., Murphy, A., Nudleman, E.,
855 Daneman, R., and Goldberg, J.L. (2019). Cholinergic neural activity directs retinal layer-specific
856 angiogenesis and blood retinal barrier formation. Nat Commun *10*, 2477.
857 Xia, C.H., Yablonka-Reuveni, Z., and Gong, X. (2010). LRP5 is required for vascular development in
858 deeper layers of the retina. PLoS One *5*, e11676.
859 Ye, X., Wang, Y., Cahill, H., Yu, M., Badea, T.C., Smallwood, P.M., Peachey, N.S., and Nathans, J. (2009).
860 Norrin, frizzled-4, and Lrp5 signaling in endothelial cells controls a genetic program for retinal
861 vascularization. Cell *139*, 285-298.
862 Yuan, J., Levitin, H.M., Frattini, V., Bush, E.C., Boyett, D.M., Samanamud, J., Ceccarelli, M., Dovas, A.,
863 Zanazzi, G., Canoll, P.*, et al.* (2018). Single-cell transcriptome analysis of lineage diversity in high-grade
864 glioma. Genome Med *10*, 57.
865 Yuan, J., and Sims, P.A. (2016). An Automated Microwell Platform for Large-Scale Single Cell RNA-Seq.
866 Sci Rep *6*, 33883.
867 Zarkada, G., Howard, J.P., Xiao, X., Park, H., Bizou, M., Leclerc, S., Kunzel, S.E., Boisseau, B., Li, J.,
868 Cagnone, G.*, et al.* (2021). Specialized endothelial tip cells guide neuroretina vascularization and blood-
869 retina-barrier formation. Dev Cell *56*, 2237-2251 e2236.
870 Zhao, Z., Nelson, A.R., Betsholtz, C., and Zlokovic, B.V. (2015). Establishment and Dysfunction of the
871 Blood-Brain Barrier. Cell *163*, 1064-1078.
872 Zhou, Z.J. (1998). Direct participation of starburst amacrine cells in spontaneous rhythmic activities in the
873 developing mammalian retina. J Neurosci *18*, 4155-4165.
874 Zuercher, J., Fritzsche, M., Feil, S., Mohn, L., and Berger, W. (2012). Norrin stimulates cell proliferation
875 in the superficial retinal vascular plexus and is pivotal for the recruitment of mural cells. Hum Mol Genet
876 *21*, 2619-2630.
877
878

880 **FIGURES AND FIGURE LEGENDS**

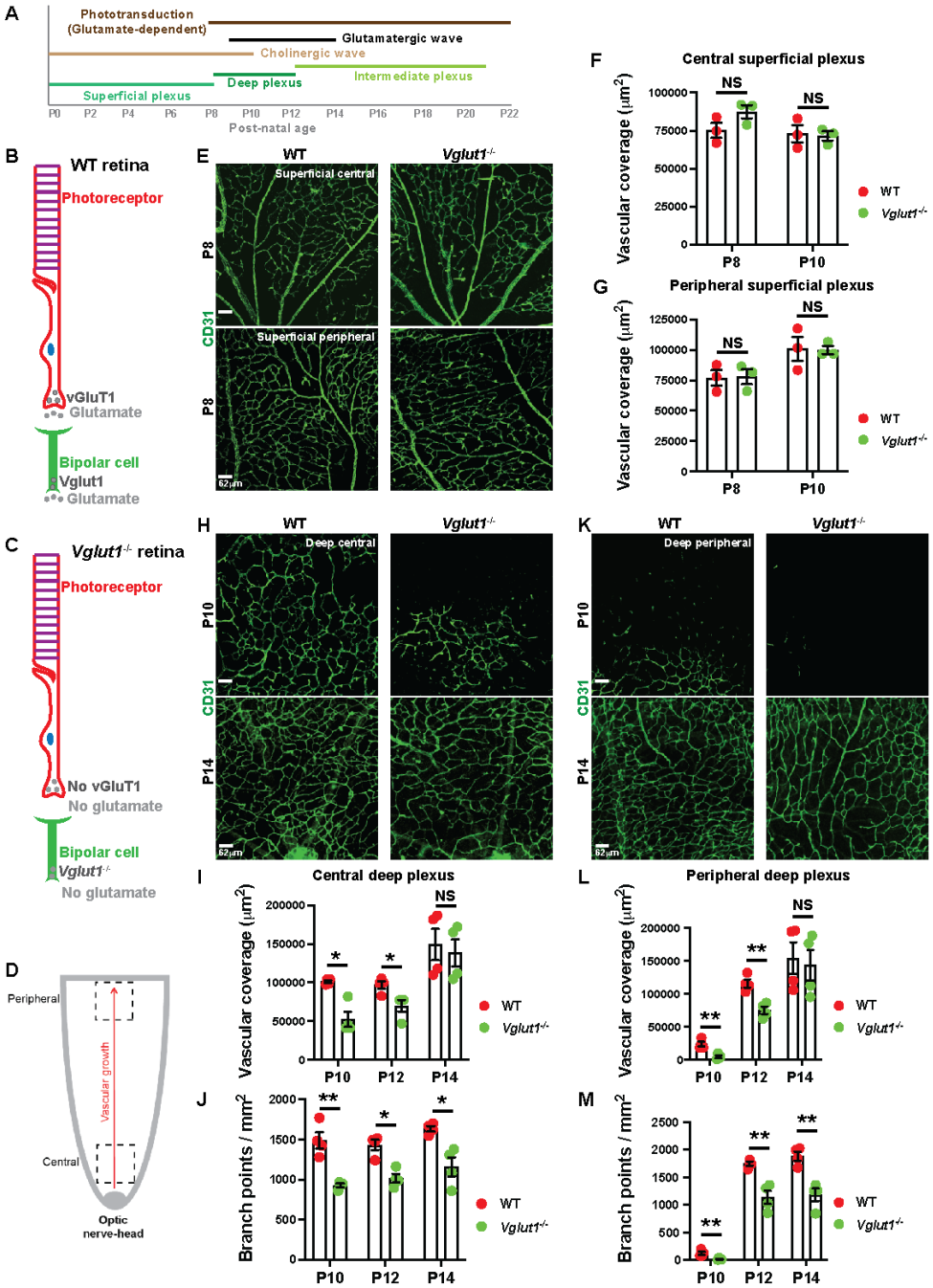

881

882 **Figure 1. Deep plexus angiogenesis is delayed in the *Vglut1*$^{-/-}$ retina. A)** Timeline of the neuronal activity
883 [cholinergic and glutamatergic waves and glutamatergic synaptic activity of photoreceptors
884 (phototransduction)] and angiogenesis (superficial, deep and intermediate plexuses) in the postnatal WT
885 retina (P1-P22). **B, C)** Schematic diagram of glutamate release from bipolar cells and photoreceptors in WT
886 (**B**) and *Vglut1*$^{-/-}$ (**C**) retinas. *Vglut1*$^{-/-}$ photoreceptors and bipolar cells fail to release glutamate into the

887 synaptic cleft. **D)** Schematic diagram of distinct developmental regions in the retina. Central retina is
888 developmentally more mature than peripheral retina. **E)** Representative images of the superficial plexus
889 from P8 WT and *Vglut1*$^{-/-}$ retinal flat-mounts stained for CD31 (green; EC marker). **F, G)** Dotted bar graphs
890 of the vascular coverage of the superficial plexus in P8 and P10 WT and *Vglut1*$^{-/-}$ central (**F**) and peripheral
891 (**G**) retina (n=3 mice/genotype). **H, K)** Representative images of the deep plexus from P10 and P14 WT
892 and *Vglut1*$^{-/-}$ retinal flat-mounts visualized with CD31 staining (green). **I, J, L, M)** Dotted bar graphs of the
893 vascular coverage (**I, L**) and branch point density (**J, M**) of the deep plexus in P10, P12 and P14 WT and
894 *Vglut1*$^{-/-}$ central (**I, J**) and peripheral (**L, M**) retina (n=4 mice/genotype). Scale bars = 62 μm. Statistical
895 analyses were done with Students t-test: *$p<0.05$, **$p<0.02$, NS = not significant. Error bars: Mean ±
896 S.E.M.
897

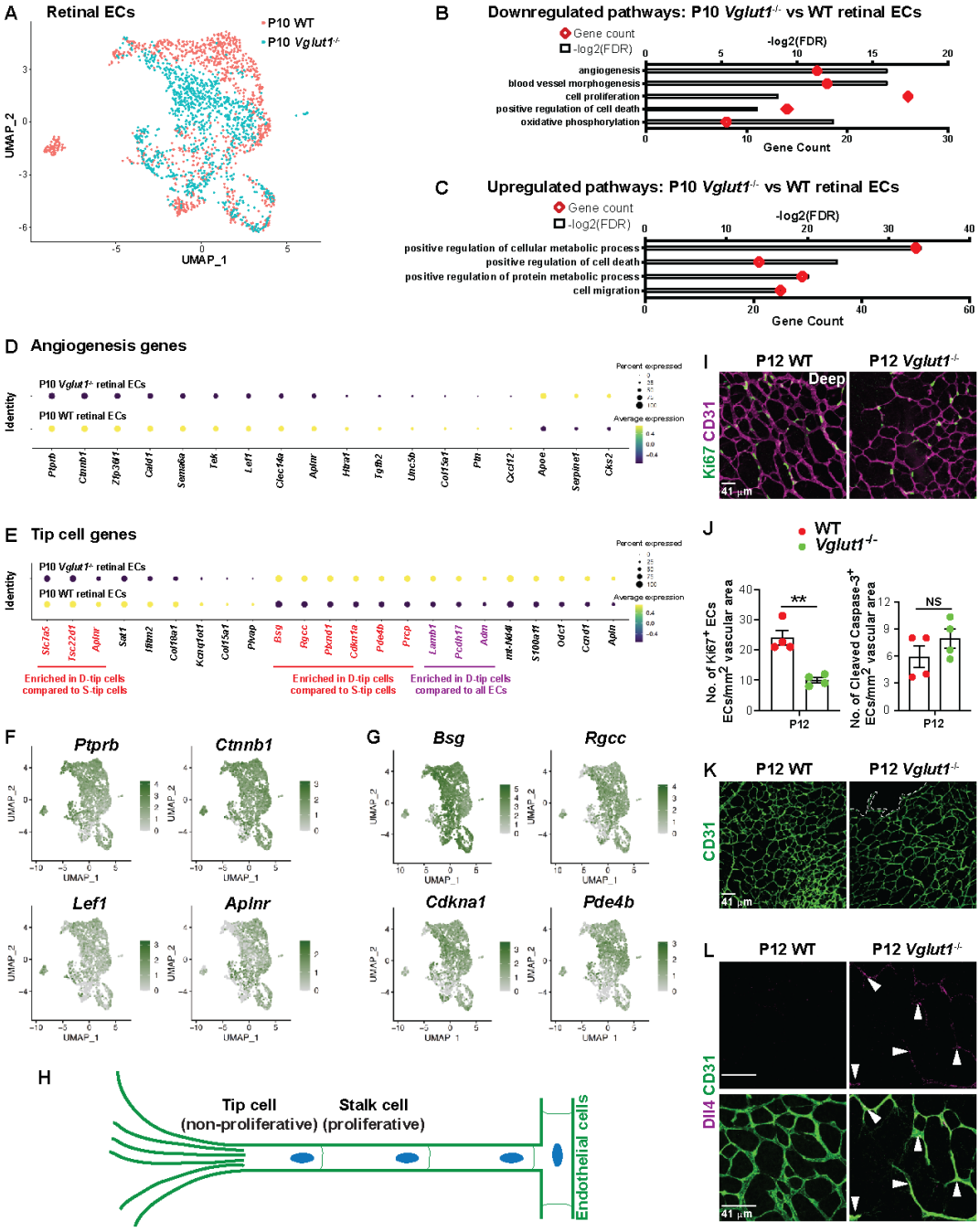

898

899 **Figure 2. Aberrant angiogenic transcriptomic signatures are present in *Vglut1*$^{-/-}$ ECs from single cell**
900 **RNA-sequencing (scRNA-seq). A)** UMAP (uniform manifold approximation and projection for dimension
901 reduction) projection shows separation of P10 WT and *Vglut1*$^{-/-}$ retinal ECs based on their transcriptomic
902 signatures. **B, C)** Gene ontology (GO) analyses of P10 WT and *Vglut1*$^{-/-}$ retinal ECs show top
903 downregulated (**B**) and upregulated (**C**) pathways. **D, E)** Dot plot of expression levels for angiogenesis (**D**)
904 and tip cell (**E**) genes in P10 WT and *Vglut1*$^{-/-}$ retinal ECs. The dot size indicates the percent of the

905 population expressing each marker; the color scale indicates the average level of gene expression. Genes
906 enriched in deep plexus tip cells (D-tip cells) compared to superficial plexus tip cells (S-tip cells) are shown
907 in red. Genes enriched in deep plexus tip cells (D-tip cells) compared to all ECs are shown in purple. **F, G)**
908 Feature plots of representative angiogenesis (**F**) and tip cells (**G**) genes in P10 WT and *Vglut1*$^{-/-}$ retinal ECs.
909 **H)** Schematic of a vascular sprout consisting of leading tip cells and proliferative stalk cells. **I)**
910 Representative images of the deep plexus from P12 WT and *Vglut1*$^{-/-}$ retinal flat-mounts stained for Ki67
911 (green) and CD31 (purple). **J)** Measurements of Ki67^{+} (proliferative) or cleaved Caspase3^{+} (apoptotic) ECs
912 in P12 WT and *Vglut1*$^{-/-}$ retinal deep plexus (*n=4*). **K)** Representative images of the deep plexus from P12
913 WT and *Vglut1*$^{-/-}$ retinal flat-mounts stained for CD31 (green). The dotted line shows the border of the
914 vascular front in the *Vglut1*$^{-/-}$ retina. **L)** Representative images of the deep plexus from P12 WT and *Vglut1*$^{-}$
915 $^{/-}$ retinal flat-mounts stained for CD31 and Dll4. Arrowheads point to Dll4^{+} tip cells in the *Vglut1*$^{-/-}$ retina.
916 Scale bars = 41 μm. Students t-test: **<0.02, NS = not significant. Error bars: Mean ± S.E.M.
917

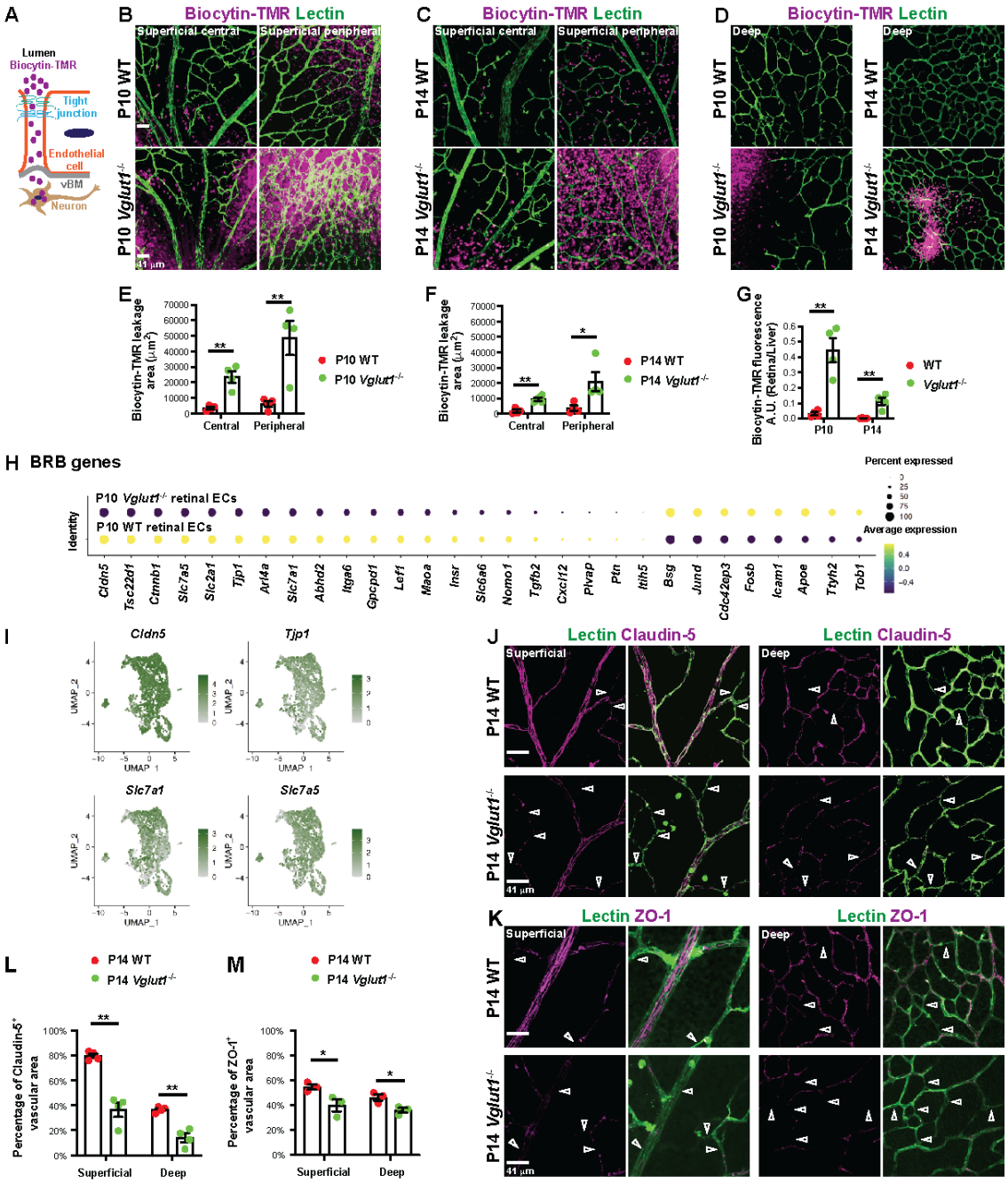

Figure 3. Paracellular BRB maturation is impaired in *Vglut1*$^{-/-}$ retina. A) Schematic of biocytin-TMR paracellular leakage through impaired tight junctions at the BRB; the leaked biocytin-TMR is taken up by neurons. vBM = vascular basement membrane. **B, C, D)** Representative images of the superficial **(B, C)** and deep **(D)** plexuses of P10 and P14 WT and *Vglut1*$^{-/-}$ retinal flat-mounts labeled with Lectin (green) 40 minutes after intravenous injection of biocytin-TMR, followed by PBS perfusion. **E, F, G)** Measurements of the area (**E, F**) and fluorescence intensity (**G**) of leaked biocytin-TMR in P10 and P14 WT and *Vglut1*$^{-/-}$

925 retinal flat-mounts (n=4). BRB formation is impaired in *Vglut1*$^{-/-}$ retina. **H)** Dot plot of expression levels
926 for BRB genes in P10 WT and *Vglut1*$^{-/-}$ retinal ECs. The dot size indicates the percent of the population
927 expressing each marker; the color scale indicates the average level of gene expression. **I)** Feature plots of
928 representative BRB genes in P10 WT and *Vglut1*$^{-/-}$ retinal ECs. **J)** Representative images of the superficial
929 and deep plexuses of P14 WT and *Vglut1*$^{-/-}$ retinal flat-mounts stained for Claudin-5 (Cldn5; purple) and
930 Lectin (green). Empty arrowheads point to Lectin^{+} blood vessels devoid of Claudin-5 at tight junctions. **K)**
931 Representative images of the superficial and deep plexuses in P14 WT and *Vglut1*$^{-/-}$ retinal flat-mounts
932 stained for ZO-1 (Tjp1, purple) and Lectin (green). Empty arrowheads point at Lectin^{+} blood vessels devoid
933 of ZO-1 localization to tight junctions. **L, M)** Measurement of Claudin-5 (**L**) and ZO-1 (**M**) coverage of
934 blood vessels in P14 WT and *Vglut1*$^{-/-}$ retinas (n=4 mice / genotype). Scale bars = 41 μm. Students t-test:
935 *<0.05, **<0.02. Error bars: Mean ± S.E.M.
936

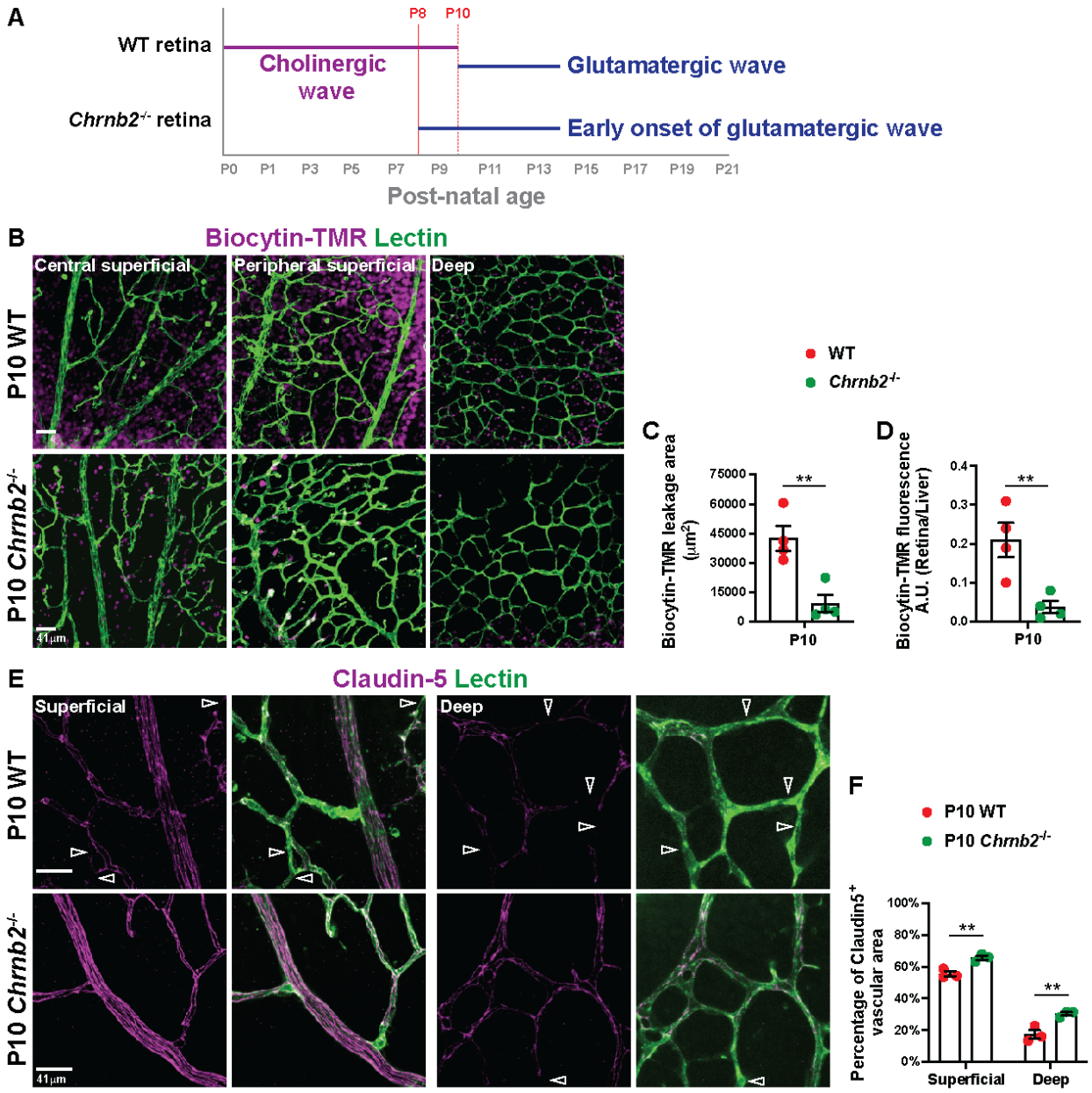

Figure 4. Paracellular BRB matures precociously in the *Chrnb2*$^{-/-}$ retina. A) Schematic diagram illustrating that glutamatergic wave begins earlier (P8) than usual (P10) in the *Chrnb2*$^{-/-}$ retina where cholinergic wave is abolished. **B)** Representative images of superficial and deep plexuses of P10 WT and *Chrnb2*$^{-/-}$ retinal flat-mounts labeled with Lectin (green) 40 minutes after intravenous biocytin-TMR injection, followed by PBS perfusion. **C, D)** Measurements of the area (**C**) and fluorescence intensity (**D**) of leaked biocytin-TMR in P10 WT and *Chrnb2*$^{-/-}$ retinal flat-mounts (n=4 mice / genotype). **E)** Representative images of the superficial and deep plexuses of P10 WT and *Chrnb2*$^{-/-}$ retinal flat-mounts

945 stained for Claudin-5 (purple) and Lectin (green). Empty arrowheads point at Lectin^{+} blood vessels devoid
946 of Claudin-5 localization to tight junctions. **F)** Measurement of Claudin-5 coverage of blood vessels in P10
947 WT and *Chrnb2*$^{-/-}$ retinas (n=3 mice / genotype). Scale bars = 41 μm. Students t-test: **<0.02. Error bars:
948 Mean ± S.E.M.
949
950
951

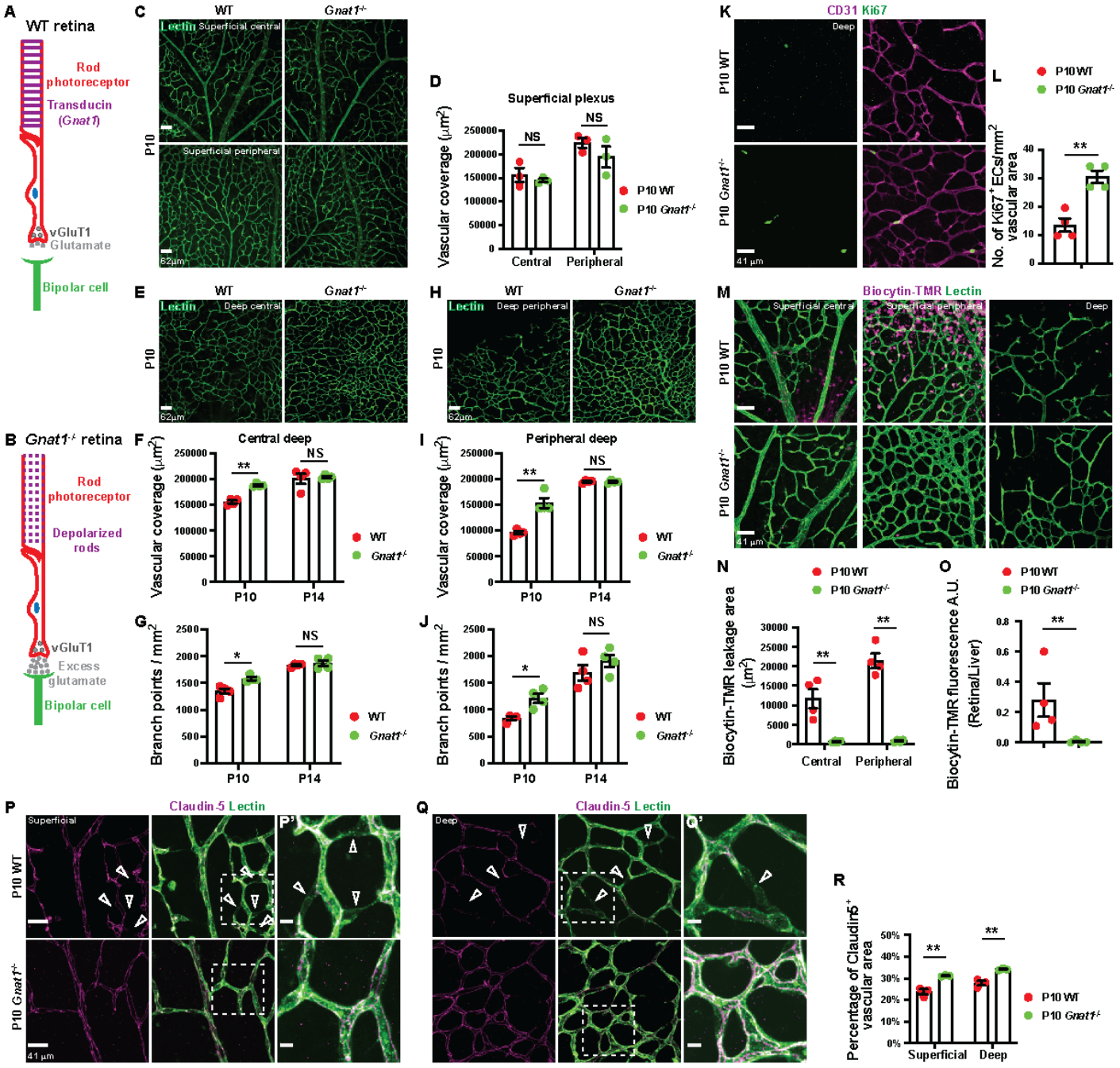

952

953 **Figure 5. Deep plexus angiogenesis and paracellular BRB maturation are accelerated in the *Gnat1*$^{-/-}$**

954 **retina. A, B)** Schematic diagrams of glutamate release from rod photoreceptors in WT (**A**) and *Gnat1*$^{-/-}$ (**B**)

955 retinas. *Gnat1*$^{-/-}$ rod photoreceptors (depolarized) release excess glutamate into the synaptic cleft. **C)**

956 Representative images of the superficial plexus in P10 WT and *Gnat1*$^{-/-}$ retinal flat-mounts stained for

957 Lectin (green). **D)** Measurements of vascular coverage of the superficial plexus in P10 WT and *Vglut1*$^{-/-}$

958 central and peripheral retina (n=3 mice / genotype). **E, H)** Representative images of the deep plexus in P10

959 WT and *Gnat1*$^{-/-}$ retinal flat-mounts stained for Lectin (green). **F, G, I, J)** Measurements of vascular
960 coverage (**F, I**) and branch point density (**G, J**) of the deep plexus in P10 and P14 WT and *Gnat1*$^{-/-}$ central
961 (**F, G**) and peripheral (**I, J**) retina (n=4 mice / genotype). **K)** Representative images of the deep plexus in
962 P10 WT and *Gnat1*$^{-/-}$ retinal flat-mounts stained for Ki67 (purple) and CD31 (green). **L)** Measurements of
963 Ki67^{+} ECs in P10 WT and *Gnat1*$^{-/-}$ retinal deep plexus (n=4 mice / genotype). **M)** Representative images
964 of superficial and deep plexuses of P10 WT and *Gnat1*$^{-/-}$ retinal flat-mounts labeled with Lectin (green) 40
965 minutes after intravenous injection of biocytin-TMR (purple), followed by PBS perfusion. **N, O)**
966 Measurements of the area (**N**) and fluorescence intensity (**O**) of leaked biocytin-TMR in P10 WT and *Gnat1*$^{-}$
967 $^{/-}$ retinal flat-mounts (n=4 mice / genotype). **P, Q)** Representative images of the superficial (**P**) and deep
968 (**Q**) plexuses in P10 WT and *Gnat1*$^{-/-}$ retinal flat-mounts stained for Claudin-5 (purple) and Lectin (green).
969 P' and Q' are magnified images of the corresponding boxed areas. Empty arrowheads point at Lectin^{+} blood
970 vessels devoid of Claudin-5 localization to tight junctions. **R)** Measurement of Claudin-5 coverage of blood
971 vessels in P10 WT and *Gnat1*$^{-/-}$ retinas (n=4 mice / genotype). Scale bars: **C, E, H** = 62 μm and **K, M, P,**
972 **Q** = 41 μm. Students t-test: *<0.05, **<0.02, NS = not significant. Error bars: Mean ± S.E.M.
973

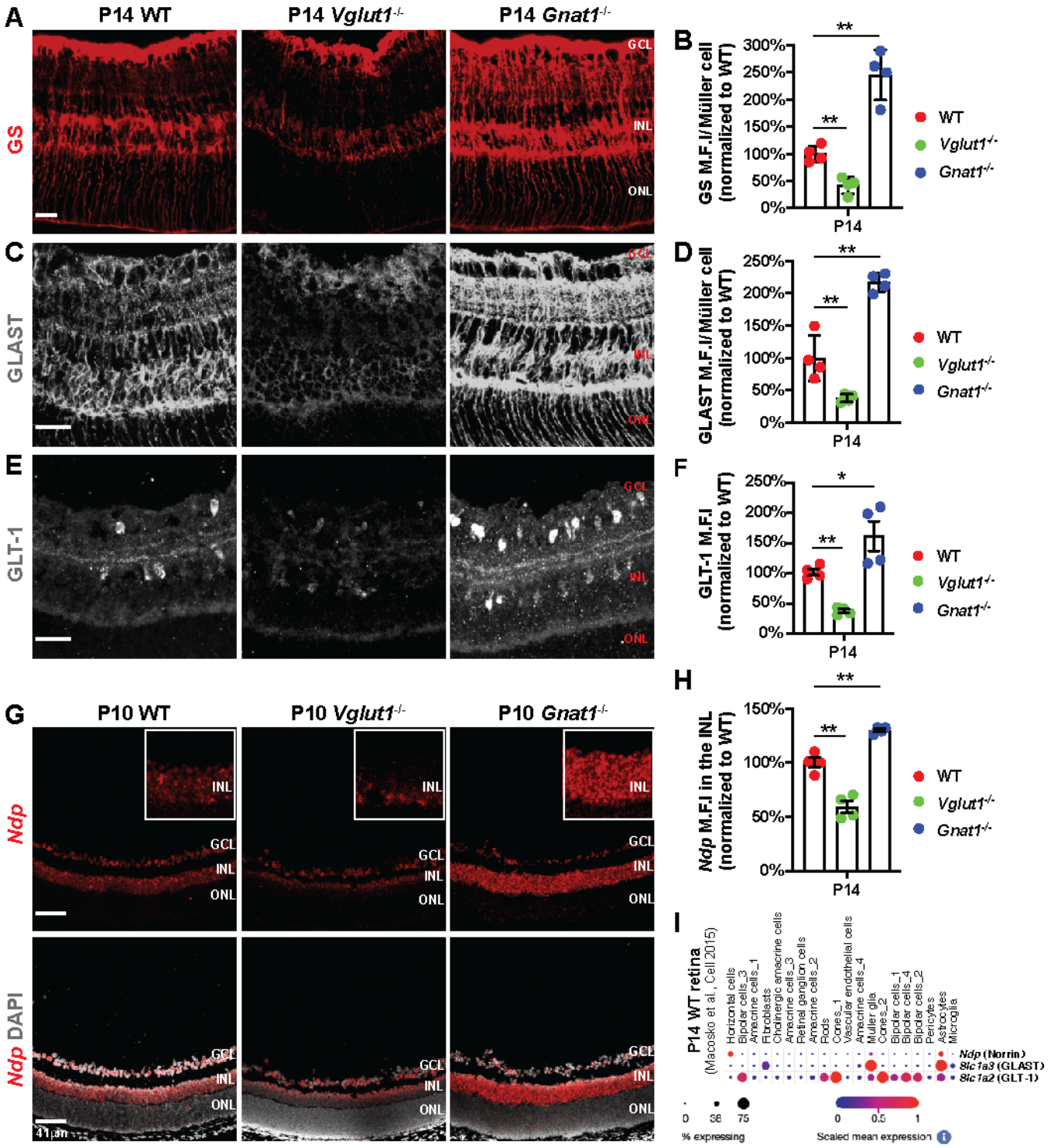

Figure 6. Expression of glutamine synthetase, glutamate transporters and Norrin are downregulated in *Vglut1*$^{-/-}$ retinas and upregulated in *Gnat1*$^{-/-}$ retinas. A, B) P14 WT, *Vglut1*$^{-/-}$ and *Gnat1*$^{-/-}$ retinal sections were stained for glutamine synthetase (GS) (**A**), and the mean fluorescence intensity (M.F.I) in the INL was quantified (**B**) for each genotype (n=4 mice / genotype). **C, D)** P14 WT, *Vglut1*$^{-/-}$ and *Gnat1*$^{-/-}$

979 retinal sections were stained for GLAST (**C**), and the M.F.I in the INL was quantified (**D**) for each genotype
980 (n=4 mice / genotype). **E, F)** P14 WT, *Vglut1*$^{-/-}$ and *Gnat1*$^{-/-}$ retinal sections were stained for GLT-1 (**E**),
981 and the M.F.I in the INL was quantified (**F**) for each genotype (n=4 mice / genotype). **G)** Fluorescent *in*
982 *situ* hybridization of P10 WT, *Vglut1*$^{-/-}$ and *Gnat1*$^{-/-}$ retinal sections with an antisense probe against *Ndp*
983 (Norrin), followed by staining with DAPI. Norrin is expressed throughout the INL. **H)** Quantification of
984 the M.F.I of *Ndp* in the INL of P10 WT, *Vglut1*$^{-/-}$ and *Gnat1*$^{-/-}$ retinal sections (n=4 mice / genotype). **I)**
985 Expression profiles of *Ndp*, *Slc1a3* (GLAST) and *Slc1a2* (GLT-1) in the P14 WT retina from an existing
986 scRNA-seq database (Macosko et al., 2015). *Ndp* mRNA is expressed predominantly by the horizontal cells
987 and Müller glia in the INL (small subsets of amacrine and bipolar cells also express *Ndp*). In the INL,
988 *Slc1a3* is primarily expressed by Müller glia and astrocytes, whereas *Slc1a2* is expressed in retinal neurons
989 as well as Müller glia. GCL: ganglion cell layer, INL: inner nuclear layer, ONL: outer nuclear layer. Scale
990 bars = 41 μm. One-way ANOVA: **<0.02, NS = not significant. Error bars: Mean ± S.E.M.
991

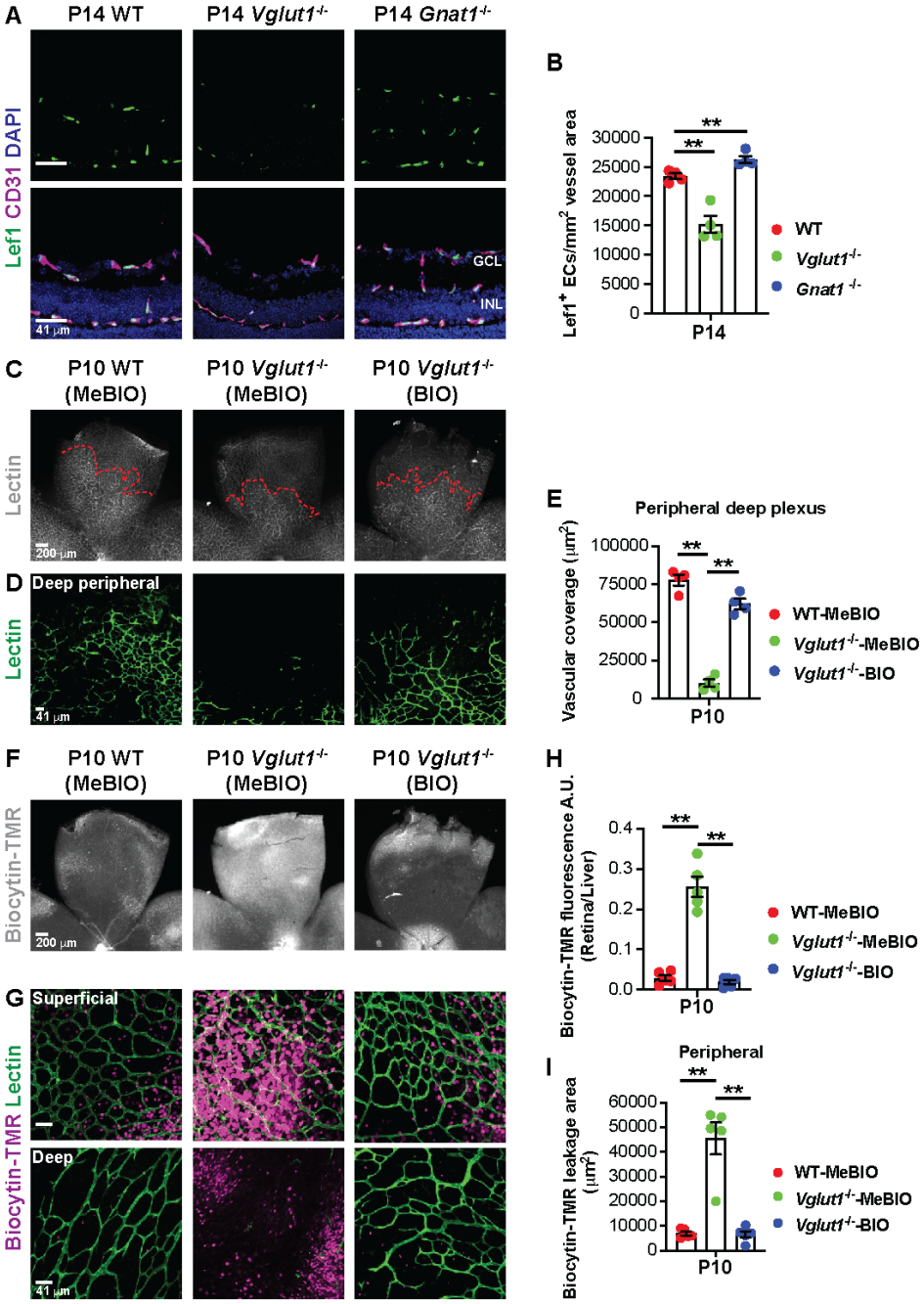

992

993 **Figure 7. Upregulation of Norrin/β-catenin signaling rescues vascular deficits of the *Vglut1*$^{-/-}$ retina.**

994 **A, B)** P14 WT, *Vglut1*$^{-/-}$ and *Gnat1*$^{-/-}$ retinal sections were stained for Lef1 (green), CD31 (purple) and

995 DAPI (blue; **A**), and the number of Lef1^{+} ECs was quantified (**B**) for each genotype (n=4 mice / genotype).

996 **C-E)** MeBIO (control)- or BIO (activates Norrin/β-catenin signaling)-treated P10 WT and *Vglut1*$^{-/-}$ retinas

997 were stained with Lectin [green; (**C**) low and (**D**) high magnification], and vascular coverage of the

998 peripheral deep plexus was quantified (**E**) for each treatment (n=4 mice / genotype). **F)** Representative

999 images of flat mount MeBIO- or BIO-treated P10 WT and *Vglut1*$^{-/-}$ retinas 40 minutes after intravenous
000 injection of biocytin-TMR and perfusion with PBS. P10 *Vglut1*$^{-/-}$ retinas treated with MeBIO (control) have
001 high leakage of biocytin-TMR in the retina. P10 *Vglut1*$^{-/-}$ retinas treated with BIO have low leakage of
002 biocytin-TMR in the retina similar to P10 WT retinas. **G**) Representative images (higher magnification) of
003 flat mount MeBIO- or BIO-treated P10 WT and *Vglut1*$^{-/-}$ retinas 40 minutes after intravenous injection with
004 biocytin-TMR (purple) and stained for lectin (green). **H, I**) Quantification of biocytin-TMR leakage area
005 (**H**) and fluorescence intensity (**I**) were quantified for each treatment (n=5 mice / genotype). GCL: ganglion
006 cell layer, INL: inner nuclear layer. Scale bars **A, D, G** = 41 μm, **C, F** = 200 μm. One-way ANOVA:
007 **<0.02. Error bars: Mean ± S.E.M.
008

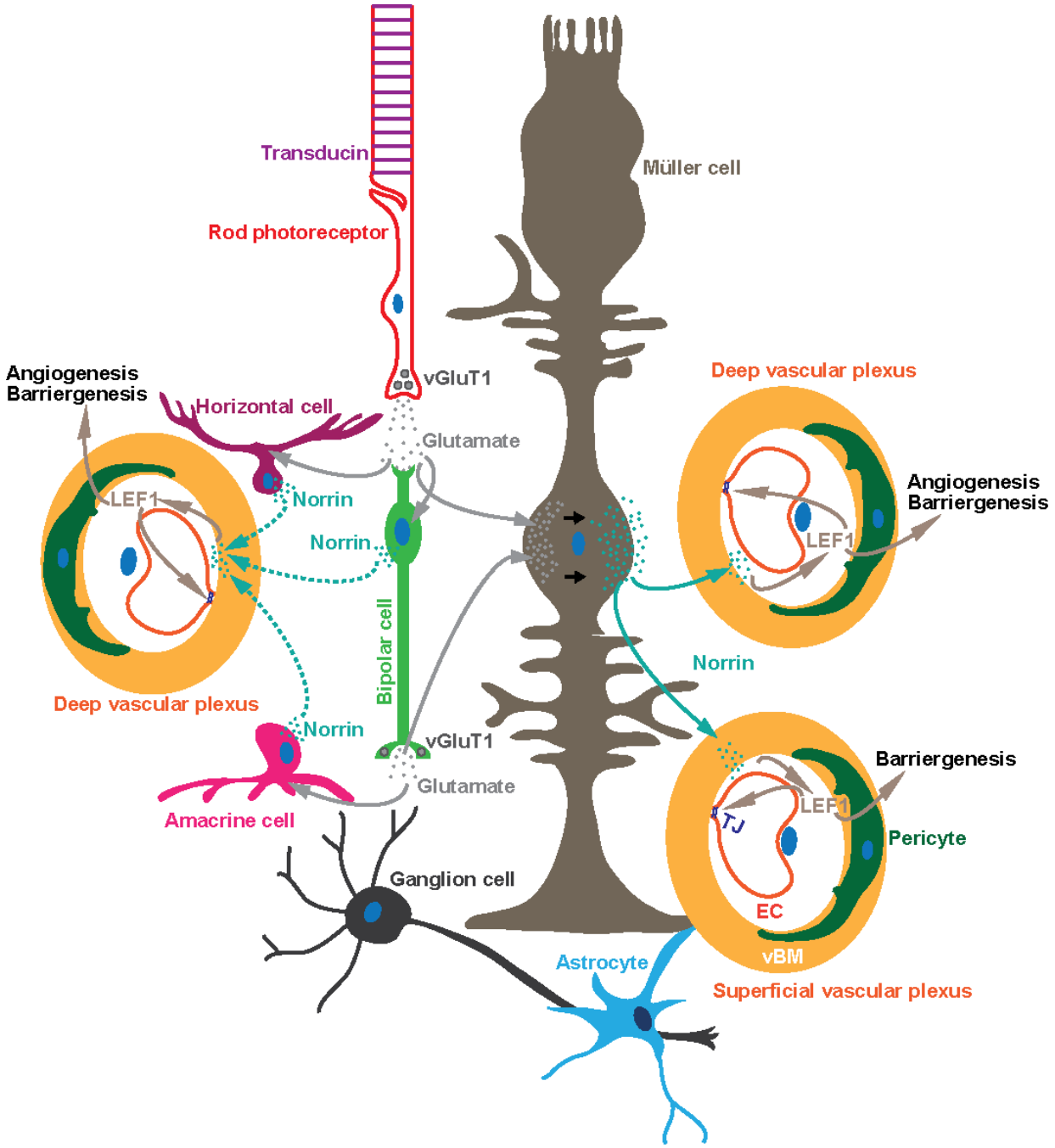

009

010 **Figure 8. Glutamatergic neuronal activity regulates retinal angiogenesis and BRB maturation**
011 **through Norrin/β-catenin signaling.** Glutamate is taken up into synaptic vesicles by vGluT1 (*Vglut1*), and
012 is released into the synaptic cleft by neurons, either during spontaneous glutamatergic wave (from bipolar
013 cells), or light-dependent glutamatergic synaptic activity of photoreceptors in the retina. The inhibition of
014 glutamate release from rods after light exposure is regulated by Transducin (*Gnat1;* purple line). The
015 released glutamate signals to Müller glia and inner nuclear layer (INL) neurons including horizontal,

016 amacrine and bipolar cells. As a result, Müller glia and INL neurons upregulate *Norrin* mRNA and protein
017 expression and likely its secretion; however, the relative contribution from Müller glia and INL neurons on
018 extracellular Norrin levels in this process is unclear. Glutamate-dependent secretion of Norrin activates
019 endothelial Norrin/β-catenin signaling, which in turn promotes deep plexus angiogenesis and the
020 paracellular BRB maturation in both the superficial and deep plexuses of the retina. INL: inner nuclear
021 layer.